AGU PUBLICATIONS

JGR

Journal of Geophysical Research: Oceans

RESEARCH ARTICLE

10.1002/2014JC010626

Key Points:
- A computational framework for sensitivity and variability of tsunami inundation
- Stochastic tsunami scenarios
- Stochastic tsunami hazard maps for hazard mapping and risk reduction

Correspondence to:
K. Goda,
katsu.goda@bristol.ac.uk

Citation:
Goda, K., T. Yasuda, N. Mori, and P. M. Mai (2015), Variability of tsunami inundation footprints considering stochastic scenarios based on a single rupture model: Application to the 2011 Tohoku earthquake, *J. Geophys. Res. Oceans*, *120*, doi:10.1002/2014JC010626.

Received 8 DEC 2014
Accepted 2 JUN 2015
Accepted article online 6 JUN 2015

Variability of tsunami inundation footprints considering stochastic scenarios based on a single rupture model: Application to the 2011 Tohoku earthquake

Katsuichiro Goda[1], Tomohiro Yasuda[2], Nobuhito Mori[2], and P. Martin Mai[3]

[1]Civil Engineering, University of Bristol, Bristol, UK, [2]Disaster Prevention Research Institute, Kyoto University, Kyoto, Japan, [3]Earth Science and Engineering, King Abdullah University of Science and Technology, Thuwal, Saudi Arabia

Abstract The sensitivity and variability of spatial tsunami inundation footprints in coastal cities and towns due to a megathrust subduction earthquake in the Tohoku region of Japan are investigated by considering different fault geometry and slip distributions. Stochastic tsunami scenarios are generated based on the spectral analysis and synthesis method with regards to an inverted source model. To assess spatial inundation processes accurately, tsunami modeling is conducted using bathymetry and elevation data with 50 m grid resolutions. Using the developed methodology for assessing variability of tsunami hazard estimates, stochastic inundation depth maps can be generated for local coastal communities. These maps are important for improving disaster preparedness by understanding the consequences of different situations/conditions, and by communicating uncertainty associated with hazard predictions. The analysis indicates that the sensitivity of inundation areas to the geometrical parameters (i.e., top-edge depth, strike, and dip) depends on the tsunami source characteristics and the site location, and is therefore complex and highly nonlinear. The variability assessment of inundation footprints indicates significant influence of slip distributions. In particular, topographical features of the region, such as ria coast and near-shore plain, have major influence on the tsunami inundation footprints.

1. Introduction

Tsunami hazard assessment involves various assumptions and approximations. Observations and data used in calibration processes are subject to errors and uncertainty. Consequently, tsunami hazard estimates for future scenarios are uncertain. From a tsunami risk management perspective, accurate assessment of tsunami hazards and quantification of uncertainty associated with the assessment are essential to mitigate and control disaster risk exposures effectively. In particular, spatial variability of tsunami hazards due to future events has important implications on tsunami resistant design of structures and evacuation planning [*Federal Emergency Management Agency* (*FEMA*), 2008; *Murata et al*., 2010]. Facing major uncertainty, assessing the sensitivity as well as variability of tsunami simulations provides valuable insights into tsunami risk reduction measures [*Geist*, 2002; *Japan Society of Civil Engineers* (*JSCE*), 2002; *McCloskey et al*., 2008; *Løvholt et al*., 2012; *MacInnes et al*., 2013; *Satake et al*., 2013; *Goda et al*., 2014].

Major components of tsunami modeling include earthquake source characterization, tsunami wave propagation, and tsunami inundation/runup. Among these, earthquake rupture is especially complex and uncertain, and is governed by prerupture stress conditions and frictional properties of the fault that are largely unknown/unobservable and heterogeneous in space. Earthquake source inversions image the space-time evolution of the rupture by matching key features of simulated data with observations. Calibration data of source inversions vary, affected by available observational networks and their recordings (e.g., strong-motion, teleseismic, geodetic, and tsunami measurements). The variability in derived earthquake rupture models can be assessed by examining an online database of finite-fault source models (SRCMOD, http://equake-rc.info/srcmod) [*Mai and Thingbaijam*, 2014], and is further quantified for the 2011 Tohoku earthquake [*Razafindrakoto et al*., 2015].

Previously, key features of multiple slip models for M_w6–8 earthquakes, each derived differently using non-uniform data and analysis methods, have been investigated by using stochastic random-field models to parameterize the complexity of earthquake slip [*Somerville et al*., 1999; *Mai and Beroza*, 2002; *Lavallée et al*.,

2006]. The stochastic method by *Mai and Beroza* [2002] is based on the spectral representation of slip heterogeneity in the wave number domain and implements the spectral synthesis to generate random fields that have realistic slip characteristics, such as asperities. Parameters of a random-field model (e.g., fractal dimension and correlation length) are related to macroscopic earthquake source features, such as moment magnitude and fault dimensions, to derive predictive models of complex earthquake slip distributions for future earthquakes that can be used for forward modeling of both strong-motion and tsunami.

Recently, the Mai-Beroza method has been extended to apply to M_w9-class megathrust subduction earthquakes by considering inversion models for the 2011 Tohoku earthquake [*Goda et al*., 2014]. The modified stochastic method is capable of modeling large slip patches along the upper segments of the fault rupture, which are responsible for causing massive tsunami and are unique features of the 2011 Tohoku event [*Fujii et al*., 2011; *Yamazaki et al*., 2011; *Gusman et al*., 2012; *Satake et al*., 2013]. It can deal with a spatial slip distribution whose slip values over a fault plane, as probability distribution, significantly deviate from the normal distribution by converting nonnormal slip values via Box-Cox transformation. The nonlinear scaling of slip values facilitates the realistic modeling of slip distribution with a heavy right-tail (i.e., relatively high-probability concentration at larger values, in comparison with the normal distribution; *Lavallée et al*. [2006]). By varying parameters of fault plane geometry and earthquake slip distributions, *Goda et al*. [2014] have conducted rigorous sensitivity analysis of global tsunami hazard measures, such as offshore tsunami wave profiles at global positioning system (GPS) wave gauges and tsunami runup height or maximum inundation. They presented the mean and coefficient of variation of tsunami inundation heights along the Tohoku coast and examined how these tsunami hazard statistics vary spatially. Their results highlight strong sensitivity of tsunami wave profiles and inundation heights to site location and slip characteristics as well as to variations in dip. Specifically, location and extent of asperities as well as topography (ria coast versus coastal plain) have significant influence on the tsunami inundation height and runup. A limitation of their study is a relatively coarse spatial resolution of bathymetry and elevation data (450 m grids), which prevents detailed assessment of inundation footprints at submunicipality levels.

The variability of the spatial extent of tsunami inundation depths in coastal cities and towns in the Tohoku region is investigated by considering different fault geometry and slip distributions. The investigations are focused upon earthquake source models that are derived from source inversion for the 2011 Tohoku event. Specifically, a source model by *Satake et al*. [2013] is employed in this paper to generate so-called stochastic tsunami scenarios with variable source parameters. For a given inverted model, source variations with different top-edge depth, strike, and fault dip as well as with stochastic slip realizations are considered (66 cases, including the original inversion model). Tsunami simulation is carried out by evaluating nonlinear shallow water equations with runup [*Goto et al*., 1997] and by considering bathymetry and elevation data with 50 m grid spacing.

Our work assesses spatial inundation processes more accurately than in previous work [*Goda et al*., 2014], thus producing more detailed tsunami hazard information at local levels. The maps of the maximum inundation depths for local communities are critically important for assessing tsunami wave forces and tsunami fragility of buildings and coastal infrastructure [*FEMA*, 2008; *Murata et al*., 2010; *Suppasri et al*., 2013]. Other important tsunami hazard parameters include the flow velocity and momentum [*Koshimura et al*., 2009; *Reese et al*., 2011]; these quantities are not subject of this study, because the inundation depth and runup are more directly observable and an extensive inundation depth/runup database is available for the 2011 Tohoku event [*Mori et al*., 2012; *Mori and Takahashi*, 2012]. Using the refined topographical data and numerous tsunami scenarios, inundation areas exceeding a depth threshold and their variability can be assessed quantitatively. For instance, depth thresholds of 2–3 m may be regarded as a critical depth for collapse and wash-away for typical wooden houses. At present, a range of spatial hazard estimates is not provided as part of scenario-based tsunami hazard and evacuation maps. Nonetheless, such information is crucial for improving disaster preparedness by understanding the consequences of different situations ("typical" versus "worst-case"), and by communicating uncertainty associated with hazard predictions [*Pang*, 2008]. The information on quantified variability is also valuable for benchmarking the prediction uncertainty for future scenarios (for which no direct observations are available).

The study is organized as follows: section 2 presents an analytical framework for assessing the sensitivity and variability of spatial and depth extent of tsunami inundation. It also summarizes a procedure for spectral analysis and synthesis of stochastic earthquake slips for M_w9-class subduction earthquakes. Section 3

presents tsunami simulation results based on stochastic slip distributions with different geometrical parameters with reference to the Satake et al. source model. Ten cities and towns in the Tohoku region are focused upon for the assessment; in particular, detailed results for Kamaishi, Onagawa, and Sendai-Natori-Iwanuma are discussed. For each location, maximum inundation depth maps are evaluated considering different scenarios and are compared with tsunami inundation/runup survey results [*Mori et al*., 2011; *Mori and Takahashi*, 2012]. In addition, the impact of key parameters (fault geometry and characteristics of asperities) on inundation depth is examined quantitatively. Finally, section 4 provides the main conclusions of this study.

2. Methodology

2.1. Framework for Tsunami Hazard Sensitivity and Variability

The sensitivity and variability of tsunami modeling results can be assessed by carrying out numerous simulations with variable key parameters and by relating relative changes of the results to the variations of the key parameters. In this study, variable earthquake source characteristics (i.e., fault geometry and slip distribution) are taken into account. (Note that there are several other aspects, such as depth-dependent rock rigidity and temporal rupture evolution, which are not evaluated within the current methodology; see section 3.1 for more details.) This means that uncertainty of initial boundary conditions for tsunami modeling is propagated through dynamical fluid systems to evaluate its impact on tsunami wave profiles and inundation depths at various locations. In such investigations, it is important to place physical constraints on the range of parameter space. For geometrical parameters, variable fault dimensions and orientations should be broadly compatible with the regional seismotectonic setting. To explore a range of possible slip distributions for a given scenario (e.g., tsunamigenic M_w9 subduction event), a slip distribution together with its spectral characteristics in the wave number domain can be specified for generating synthetic slip distributions [*Goda et al*., 2014]; the method for generating realistic earthquake slip random fields is described in section 2.2.

The source variations of a megathrust subduction earthquake can be determined as follows. Multiple inversion models or reference models for a given critical scenario are gathered from the literature. For instance, *Goda et al*. [2014] considered 11 source models that are developed using teleseismic/tsunami/geodetic data to constrain the slip distribution over the fault plane. When different inversion models are considered, not only geometrical and slip parameters but also dimensions and locations of the fault plane can be altered. Consequently, details of the slip distribution and fault geometry, such as location, size, shape, and amplitude of asperities, differ significantly among the inversion models, reflecting the complexity and uncertainty of the rupture process of megathrust subduction earthquakes. The adopted inversion models are treated as a reference to further produce models with variable source characteristics. For a given source model, depth to the top of the fault plane, strike angle, and dip angle are varied with respect to the original model. The ranges of geometrical parameters are chosen based on regional seismotectonic setting. For geometrical features, only one parameter is changed at a time while the slip distribution of the original model is retained. Therefore, the results are useful for evaluating the sensitivity of these parameters sequentially.

On the other hand, locations and amplitudes of asperities, which have major influence on tsunami modeling, are not completely controlled by slip parameters (e.g., Hurst number, correlation length, and Box-Cox power parameter; see section 2.2), because random variables are involved in stochastic slip modeling. Slip values over the fault plane are dependent one another to satisfy the total seismic moment constraint and the specified spatial heterogeneity. Therefore, a standard one-at-a-time sensitivity analysis is not applicable. Multiple realizations of a target slip distribution are generated from an earthquake slip model, parameters of which are determined for a given original slip model. Using the tsunami simulation results from multiple stochastic slip distributions, the variability of tsunami hazard estimates due to slip variations can then be assessed. Furthermore, by repeating the same analysis for different reference models, a wide range of possible source models for the specified scenario can be explored to quantify their effects on tsunami wave heights and coastal inundation.

It is important to emphasize that stochastic source models are generated by considering a wide range of possible variations of earthquake source characteristics for a broadly defined scenario that may be applicable to tsunami hazard mapping purposes. In this study, the 2011 Tohoku earthquake is focused upon for

two reasons. First, numerous tsunami (as well as seismic/geodetic) observations are available for this event and they can be used for comparing a range of possible tsunami hazard predictions with the observations from retrospective viewpoints. Second, the generated source models can be used to assess the sensitivity and variability of tsunami hazard parameters from prospective viewpoints. Recognizing that different inversion models reflect different aspects of physical rupture processes during the 2011 Tohoku earthquake, a set of earthquake source models that have been developed by different researchers using different methods and data can be adopted to characterize a certain aspect of epistemic uncertainty related to source modeling. In this study, a single reference source model for the 2011 Tohoku earthquake (i.e., Satake et al. model) is considered; results based on multiple source models are reported elsewhere.

A set of synthesized earthquake source models is useful for two applications. The first application is to refine existing source inversion models in comparison with various tsunami observations from retrospective perspectives. Typically, tsunami inversion is formulated as a constrained linear inversion problem by utilizing offshore wave/deformation measurements and tidal gauge recordings [*Satake et al*., 2013]. Inland inundation/runup survey data usually are not used directly in the inversion, but are employed for validating the developed model, retrospectively. One of the most widely applied metrics for such assessment is the K and κ factors [*Aida*, 1978]:

$$\log_{10} K = \frac{1}{n}\sum_{i=1}^{n} \log_{10} H_{obs,i}/H_{simu,i}, \tag{1}$$

and,

$$\log_{10} \kappa = \sqrt{\frac{1}{n}\sum_{i=1}^{n} (\log_{10} H_{obs,i}/H_{simu,i})^2 - (\log_{10} K)^2}, \tag{2}$$

where n is the number of data points, and H_{obs} and H_{simu} are the observed and simulated tsunami hazard values, respectively. Essentially, the K factor is the geometric mean of the ratio between the observed and simulated inundation/runup heights, while the κ factor is the logarithmic standard deviation of the ratio. *JSCE* [2002] suggests that a suitable tsunami source model should achieve the K factor between 0.95 and 1.05, with a κ factor of less than 1.45. The proposed criteria may not be directly applicable to the comparisons of simulated and observed tsunami inundation depths of this study, because dense spatial features of the inundation depths within cities and towns along the Tohoku coast are considered. In contrast, previous validation studies [e.g., *Shuto*, 1991; *JSCE*, 2002] look at much more sparse features of the tsunami inundation heights (e.g., a few points for each location). Using numerous realizations of candidate source models (which reflect the key source features of the seismic event of interest), a set of source models that have small errors with respect to the observations can be identified. From an inversion perspective, this can be regarded as a two-stage nonlinear source inversion method. The refined inversion models can explain both linear and nonlinear physical processes of tsunami wave propagation and inundation.

The second application of stochastic source models is assessing the variability of tsunami simulations with respect to the slip distribution, as well as the development of stochastic tsunami scenarios and stochastic inundation maps. In this context, all models may be treated equally, although some models perform better than others when compared with some observations. It is noteworthy that for future tsunami scenarios, a priori performance tests of individual models are not always feasible. The information of the range of possible tsunami hazard estimates, which should also contain unexpected or extreme events, is useful for hazard mapping, uncertainty communication, and emergency preparedness.

It is instructive to view the above mentioned stochastic approach for major tsunami scenarios from probabilistic tsunami hazard analysis (PTHA) methodology [*Geist and Parsons*, 2006; *Thio et al*., 2007; *Horspool et al*., 2014]. The difference between the stochastic scenario method and the PTHA is that the former focuses upon the spatial variability of source characteristics for a specified scenario, whereas the latter defines numerous tsunami sources (both far-field and near-field) that may affect a site of interest significantly and evaluating the relative contribution to the overall tsunami hazard. These two approaches are complementary and eventually, they should be integrated into a more comprehensive methodology, as suggested by *Horspool et al*. [2014] who have taken into account random variability of slip distribution (without spatial dependency of slips). It is noteworthy that the extension of the stochastic scenario method

requires the consideration of multiple different scenarios having a wide range of earthquake magnitudes. In this regard, recently developed magnitude-size relationships are useful [*Murotani et al*., 2013]. A major challenge that needs to be dealt within PTHA is the determination of the maximum earthquake magnitude, which involves considerable uncertainty [*Kagan and Jackson*, 2013].

2.2. Spectral Analysis and Synthesis of Earthquake Slip Models

An earthquake slip modeling procedure, which is based on spectral analysis of an inversion-based source model and spectral synthesis of random fields, generates earthquake slip distributions with statistical properties equivalent to the inverted source model. The method is based on *Mai and Beroza* [2002], and has been modified for large megathrust subduction earthquakes [*Goda et al*., 2014]. The random-field generation method is designed to balance similarity in key features of the inversion-based models (e.g., overall probabilistic characteristics of slip values over a fault plane and its spectral characteristics) with dissimilarity of fine details (e.g., locations of large slip patches). A graphical flowchart of the procedure is shown in Figure 1; an example shown in the figure is for the Satake et al. model.

Prior to spectral analysis, an original slip model needs modifications (STEP 1). An original slip model is read as a cell-based distribution; in this step, an asperity zone, which is used for pattern matching in spectral synthesis, is identified (STEP 1-1). The asperity zone is defined as a set of subfaults that have slip values greater than a specified threshold value. Typically, the threshold is set to two to three times the average slip [*Somerville et al*., 1999; *Mai et al*., 2005]. One of the key features of the slip models for the 2011 Tohoku earthquake is that very large slip values (e.g., exceeding 40 m) are obtained for a small number of subfaults (note: the average slips are approximately 10 m) [*Goda et al*., 2014]. This results in slip values on the fault plane whose overall distribution is significantly different from the normal distribution and exhibits a heavy right-tail feature (in comparison with the normal distribution with the same statistics; see STEP 1–2). This can cause problems in stochastic simulation of slip distributions because the random-field method implemented in this study [*Pardo-Iguzquiza and Chica-Olmo*, 1993] generates slip distributions with quasi-normal slip values over a fault plane (note: they have specified spatial heterogeneity of earthquake slips). To deal with nonnormal distribution of slip values, nonlinear scaling of the slip values is considered in the random-field generation procedure (see STEP 3). To identify a suitable nonlinear scaling method, in STEP 1–2, characteristics of the slip values over a fault plane are analyzed using the Box-Cox transformation, in which an original variable x (i.e., nonnormal slip values) is converted into y as: $y = (x^{\lambda} - 1)/\lambda$. The method identifies the best power transformation parameter λ by maximizing the linear correlation coefficient between the transformed variable y (of the slip values) and the standard normal variate for different values of λ. For the Satake et al. model, an optimal value of λ is estimated as 0.2 (STEP 1–2). The obtained value of λ is used to perform nonlinear scaling of the synthesized slip distributions in spectral synthesis (i.e., inverse Box-Cox transformation; STEP 3). Subsequently, the cell-based model is converted to a grid-based model and interpolated bilinearly, and is then tapered by adding three rows and columns over which slip decreases to zero to each side of the fault plane to achieve smooth transition at the fault boundary (STEP 1–3). The grid spacing for interpolation is selected according to the grid size of the original slip model.

Using the interpolated and tapered slip distribution in STEP 1, fast Fourier transform (FFT) of the slip distribution is carried out to obtain the two-dimensional (2-D) normalized power spectrum (STEP 2-1). Usable wave number ranges are determined based on the characteristic dimension of the fault plane for the lower limit and the spatial resolution of the original slip model for the upper limit. The extracted normalized power spectra in the downdip and along-strike directions are fitted by the power spectrum of a theoretical autocorrelation function (STEP 2-2; see *Mai and Beroza* [2002] and *Goda et al*. [2014] for further details). In this study, the power spectrum $P(k)$ of an anisotropic von Kármán autocorrelation function is considered:

$$P(k) \propto \frac{A_x A_z}{(1+k^2)^{H+1}}, \tag{3}$$

where k is the wave number, $k = (A_z^2 k_z^2 + A_x^2 k_x^2)^{0.5}$, A_z and A_x are the correlation lengths for the downdip and along-strike directions, respectively, and H is the Hurst number. At wave number scales greater than the correlation length, the slip distribution is mainly governed by the average slip characteristics, whereas at wave number scales less than the correlation length, local heterogeneity dominates. A_x and A_z control the absolute level of the power spectrum in the low wave number range (i.e., $k \ll 1$) and capture the

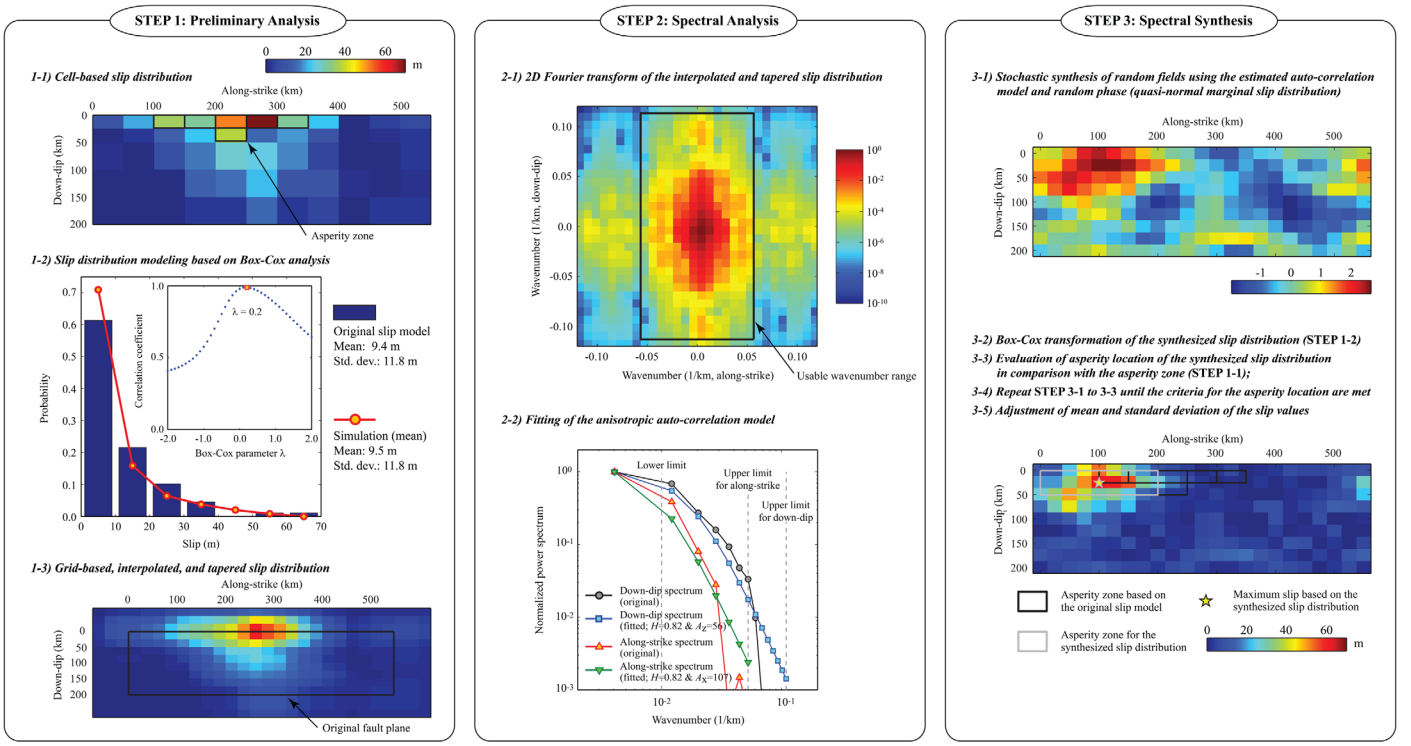

Figure 1. Spectral analysis and synthesis of stochastic earthquake slip.

anisotropic spectral features of the slip distribution. H determines the slope of the power spectral decay in the high wave number range, and is theoretically constrained to fall between 0 and 1. In equation (3), smaller values of H generate more heterogeneous slip model, while $H \sim 1.0$ produces smooth slip distributions. For $H = 0.5$, equation (3) represents the power spectrum of the exponential distribution. For the Satake et al. model, A_x and A_z are estimated as 56 and 107 km, respectively, and $H = 0.82$. The estimated correlation lengths are greater than those for events analyzed in *Mai and Beroza* [2002]. This is expected because the correlation length scales with the earthquake magnitude (or characteristic dimensions) [*Mai and Beroza*, 2002].

In STEP3, multiple realizations of slip distributions with desired stochastic properties are obtained. First, a random field, having quasi-normal distribution with a desired spatial correlation structure, is synthesized using a Fourier integral method (STEP 3-1) [*Pardo-Iguzquiza and Chica-Olmo*, 1993]. The amplitude spectrum of the target slip distribution is specified by the theoretical power spectrum with the correlation lengths and Hurst number that are estimated in STEP 2, while the phase spectrum is represented by a random phase matrix. The constructed complex Fourier coefficients are transformed into the spatial domain via 2-D inverse FFT. Note that the synthesized slip distribution is not tapered. The synthesized slip distribution is then scaled nonlinearly to have heavy right-tail characteristics using the Box-Cox parameter λ estimated in STEP 1–2 (STEP 3-2). In this manipulation, an upper bound (i.e., maximum slip of the original model) is implemented for the transformed slip distribution to avoid unrealistically large slip.

To resemble the synthesized slip distribution with the original one in terms of location and amplitude of asperities, a rectangular asperity zone is defined for the synthesized slip distribution, and then compared with the original slip distribution. The asperity dimensions of the synthesized distribution are specified by fractions of fault length and width, whereas the extent of the slip concentration around the asperity is specified by a percentage of slip within the asperity zone with respect to the total sum of slip over the fault plane. Parameters of the rectangular asperity zone are determined based on the original slip model [see *Goda et al.*, 2014, for further details]. For the Satake et al. model, the dimensions of the asperity zone are set to 50 and 220 km for the downdip and along-strike directions, respectively (in terms of fault dimensions,

these correspond to fractional factors of 0.25 and 0.4, respectively), whereas the slip concentration ratio of 0.3 is considered. These parameters approximately resemble the asperity zone that is identified for the original slip distribution (STEP 1-1). An acceptable slip distribution is required to have its maximum slip patch within the asperity zone of the original distribution, with its slip concentration located in the rectangular asperity zone greater than a threshold value defined based on the original slip distribution (STEP 3-3). To ensure this requirement, multiple realizations are generated (STEP 3–4). Finally, the mean and standard deviation of the transformed slip distribution are adjusted to achieve similar statistics of the synthesized slip model with regards to the original slip model. To allow some variation of the slip statistics (i.e., seismic moment), random multiplication factors for the mean and standard deviation are generated from the uniform distribution with lower and upper limits and are used to determine the target slip statistics. In this study, the lower and upper limits of the random multiplication factors for the mean and standard deviation are set to minus and plus 5% with respect to the target slip statistics based on the original slip distribution. The value of 5% is selected arbitrarily and is less than variation of the slip statistics among different published source models [*Goda et al*., 2014]. Because the target slip statistics for the Satake et al. model are 9.43 m for the mean and 11.75 m for the standard deviation, respectively, slip statistics of the synthesized slip distributions take values between 8.96 and 9.90 m for the mean and values between 11.16 and 12.34 m for the standard deviation, respectively. For each acceptable slip distribution (which passes STEP 3–4), target slip statistics are sampled from ranges between 8.96 and 9.90 m and between 11.16 and 12.34 m for the mean and standard deviation, respectively, and then the synthesized slip distribution is scaled to achieve these target slip statistics.

3. Sensitivity and Variability of Inundation Footprints

3.1. Tsunami Inundation Simulations Based on the Satake et al. Model

Tsunami modeling is carried out using a well-tested numerical code [*Goto et al*., 1997] that is capable of generating offshore tsunami propagation and inundation profiles by evaluating nonlinear shallow water equations with runup using a leapfrog staggered-grid finite difference scheme. The inundation and runup calculations are performed by a moving-boundary approach of *Iwasaki and Mano* [1979] at the water front, where a dry or wet condition of a computational cell is determined based on total water depth, taking into account bottom friction by Manning's formula. The mass and momentum flux of inland propagation of tsunami waves are strongly dependent on local water depth and bottom friction. Therefore, accuracy of the numerical results depends on spatial resolution. The computational domains are nested at four resolutions from fault rupture to land (i.e., 1350, 450, 150, and 50 m domains). Computational cells include those on land, and coastal defense structures (e.g., breakwaters) within a cell are taken into account using overflowing formulae as a subgrid model.

For simulating the 2011 Tohoku tsunami, information on bathymetry/elevation, roughness, and coastal defense structures is obtained from the Cabinet Office of the Japanese Government. The ocean-floor topography data are based on the digital bathymetry data and nautical charts developed by Japan Hydrographic Association and Japan Coastal Guard. The land elevation data are based on the 50 m grid digital elevation model (DEM) developed by the Geospatial Information Authority of Japan. The raw data are the standard 1:25,000 topographical map of Japan and are obtained from aerial photographic surveys. It is noteworthy that the 50 m grid DEM data, which only represent an average value for a given cell, are rough approximations of the elevations at individual sites. The bottom friction is evaluated using Manning's formula. Four Manning's coefficients are assigned to computational cells based on national land use data in Japan (100 m mesh): 0.02 $m^{-1/3}$ s for agricultural land, 0.025 $m^{-1/3}$ s for ocean/water, 0.03 $m^{-1/3}$ s for forest vegetation, and 0.04 $m^{-1/3}$ s for urban areas. It is noted that the assigned roughness coefficients are crude representation of actual situations and depend on the data resolution. When fine-resolution data (e.g., 5 m or less) are used, the roughness coefficients should be adjusted accordingly to simulate tsunami inundation processes accurately [*Kaiser et al*., 2011].

To compute initial water surface elevation for an earthquake slip model, analytical formulae for elastic dislocation by *Okada* [1985] together with the equation by *Tanioka and Satake* [1996] are used. The latter is to take into account the effects of horizontal movements of steep seafloor on the vertical water dislocation. The effects of hydrodynamic response of water column are not taken into account; ignoring the

hydrodynamic effect results in high content of short wavelength components of waves at tsunami sources [*Kajiura*, 1963; *Løvholt et al*., 2012; *Glimsdal et al*., 2013]. In this study, the Satake et al. source model is considered as a reference. The fault rupture is assumed to occur instantaneously. For the Satake et al. model, ignoring the time-dependent rupture process [*Hooper et al*., 2013] leads to the generation of short wavelength components of waves because the rupture process of the 2011 Tohoku earthquake is completed over a relatively long duration (300 s), involving a few episodes with large slips [*Satake et al*., 2013; *Goda et al*., 2014]. The significant effects are also attributed to the zero top-edge depth of the Satake et al. model, resulting in sharp discontinuity of vertical deformation profiles along the Trench. This simplification was considered in this study because stochastic source modeling methods for temporal rupture evolution are not fully developed and some of the source models adopted by *Goda et al*. [2014] are based on instantaneous rupture representation. Numerical tsunami calculation is performed for duration of 2 h with an integration time step of 0.5 s.

The source model by *Satake et al*. [2013] was developed by inverting 11 ocean-bottom pressure gauge measurements, 10 offshore GPS wave gauge data, and 32 tidal wave gauge data along the coastline. Figure 2a shows the source model and the calculated vertical deformation contours using the Okada equations and the Tanioka-Satake equation. The Satake et al. model places large slip patches along the Japan Trench; the largest patch has a slip of 69 m, which is accumulated over the entire rupture process of 300 s. The large slip features along the Trench can be clearly seen in the vertical deformation contour. Another important feature of the Satake et al. model is that a relatively large slip patch ($\approx$30 m) is placed in the northern part of the Tohoku region, which generates large tsunami waves in central/northern Iwate Prefecture, in comparison with other source models [*Goda et al*., 2014]. Physically, the large slip patch may be an artifact by mapping the effects of a large local submarine landslide into the slip inversion [*Ichinose et al*., 2013; *Tappin et al*., 2014]. Figure 2b shows the maximum tsunami wave height contours based on the original Satake et al. model (note: filled 2-D contours are based on the maximum tsunami wave height values calculated at specified grid points). The results indicate that the simulated tsunami waves are particularly large off northern Miyagi Prefecture and southern/central Iwate Prefecture (note: yellow-to-red color represents the maximum tsunami wave heights of 12 m or greater). The large tsunami waves in northern Iwate Prefecture are caused by the large slip patch along the Trench off Iwate Prefecture.

The Satake et al. model has constant top-edge depth and strike angle of 0 km and 193°, respectively, whereas its dip angle varies from 8° to 16° (dip increases as a fault segment becomes deeper). When the original source model has variable geometrical parameters over the fault plane, the average value of the parameters is used to define a reference case. Hence, for the Satake et al. model the reference dip angle is set to 10.8°. In assessing the sensitivity and variability of inundation depths, geometrical parameters of the reference source model are varied, and multiple slip distributions are generated using the stochastic approach of section 2.2. More specifically, the depth to the top of the fault plane is changed by -2.5, $+2.5$, $+5$, $+7.5$, and $+10$ km with respect to the reference top-edge depth (depth shift is defined as positive downward); the strike angle is varied by $-5°$, $-2.5°$, $+2.5°$, $+5°$, and $+7.5°$ with respect to the reference strike; and the dip angle is changed by $-2.5°$, $+2.5°$, $+5°$, $+7.5°$, and $+10°$ from the reference dip. Note that the top-edge depth shift of -2.5 km is not applicable to the shallowest part of the Satake et al. source model along the Japan Trench because the top-edge depth is set to 0 km. One important issue that is not taken into account in varying the top-edge depth of the fault plane is the consideration of depth-dependent rock rigidity. Typically, rock rigidity increases with depth [*Bilek and Lay*, 1999] and thus it affects the crustal deformation due to earthquake rupture. The effects due to variable rock rigidity on tsunami simulation can be significant [*Geist and Bilek*, 2001]. Nonetheless, constant rigidity is adopted to be consistent with the source inversion analysis carried out by *Satake et al*. [2013]. For stochastic slip scenarios, 50 realizations of a target slip distribution are generated. The simulated slip distributions have similar spatial characteristics to the original slip model but have different asperity characteristics.

The variability of inundation along the Tohoku coast is therefore evaluated by considering 66 scenarios (including the original source model). To facilitate the comparison of spatial and depth extent of simulated inundation with actual inundation/runup observations from the 2011 Tohoku Tsunami Joint Survey (TTJS) [*Mori et al*., 2011; *Mori and Takahashi*, 2012], 10 strongly affected cities and towns in the Tohoku region [*Fraser et al*., 2013] are considered. The zoomed plot in Figure 2b shows the locations of the 10 cities and towns (from North to South): Miyako, Kamaishi, Ofunato, Rikuzentakata, Kesennuma, Onagawa, Ishinomaki-Higashimatsushima, Shiogama-Shichigahama, Sendai-Natori-Iwanuma, and Watari-Yamamoto-Soma. In the

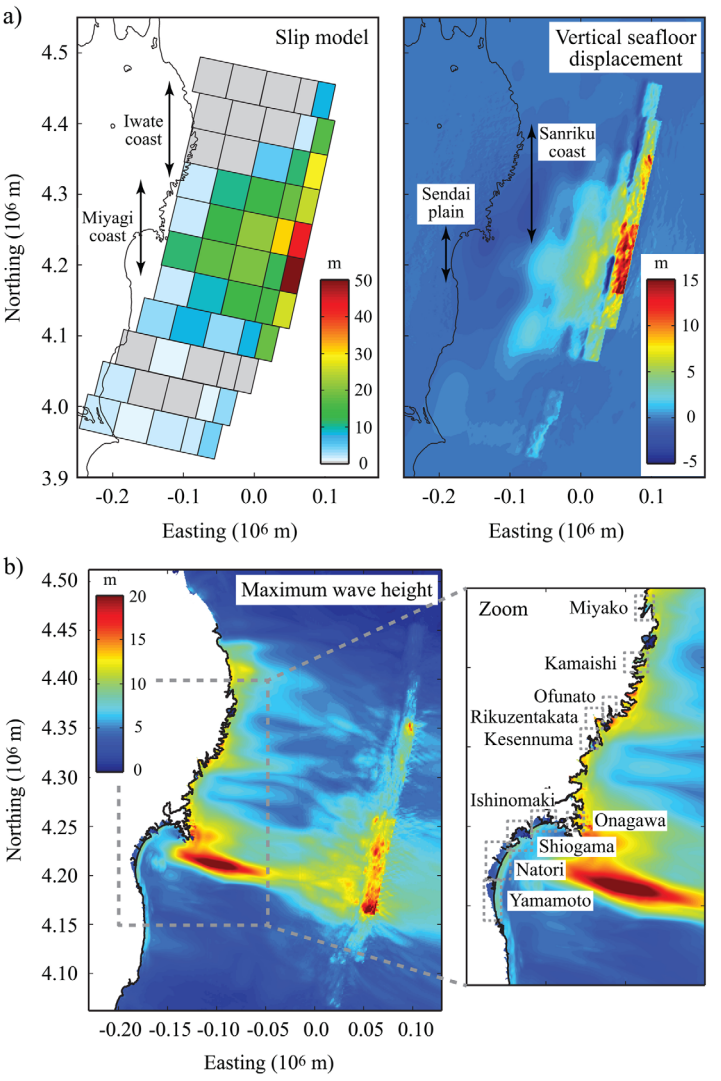

Figure 2. (a) Slip distribution and vertical seafloor displacement based on the Satake et al. model, and (b) maximum wave height contours and locations of 10 cities and towns.

following, detailed tsunami simulation results for Kamaishi, Onagawa, and Sendai-Natori-Iwanuma are discussed in sections 3.2–3.4, respectively, while combined results for the 10 cities and towns are discussed in section 3.5. The selected three locations, i.e., Kamaishi, Onagawa, and Sendai-Natori-Iwanuma, for the detailed results are in central Iwate Prefecture, northern Miyagi Prefecture, and central Miyagi Prefecture, respectively. The first two are positioned in the Sanriku ria coast, whereas the latter is located in the Sendai coastal plain. Because the large slip patches and epicenter are located off northern Miyagi Prefecture, the tsunami wave propagation from the source region for Kamaishi and Onagawa is different.

The simulated inundation depths are obtained from the tsunami simulations by subtracting the DEM data from the calculated tsunami inundation heights for the same computational cells. The reference elevation of the tsunami inundation height is the Tokyo Peil (T.P.), and simulation results are not adjusted for the local tidal levels. The DEM data used for height adjustment are those provided by the Cabinet Office (50 m grids). The TTJS data are the inundation height with respect to T.P. [*Mori et al.*, 2011]; thus they also need to be converted to the inundation depth, measured from the ground. The 50 m grid DEM data from the Cabinet Office are used for correcting the elevation of the measured TTJS inundation heights. The differences between the DEM and the actual elevation can be large especially at steep hills. Therefore, some of the corrected TTJS data may be inaccurate, which should be taken into account in interpreting the results presented below. The main reason for adopting inundation depth, rather than inundation height, is to evaluate the variability and sensitivity of tsunami hazard measures that are more directly related to tsunami risks at individual sites. For instance, when inundation depth is integrated with tsunami fragility curves [*Suppasri et al.*, 2013], tsunami damage assessment for individual properties can be carried out.

The simulation results are compared with the TTJS observations, and various summary statistics of the simulated inundation depths are computed for such purposes. The mean and standard deviation of the inundation depths for the 10 locations are listed in Table 1, noting that the table only shows the cases where inundation depth contours are presented for the detailed results in sections 3.2–3.4. The comparison facilitates the identification of the source model that achieves the minimum sum of squared errors (MinSSE) between the simulation and the observations for a given location. Other summary statistics used in this

Table 1. Inundation Depth Statistics (Mean and Standard Deviation in Meters) for the Satake et al. Model

City/Town	TTJS	Satake et al. Model	Depth = −2.5 km	Depth = +10 km	Strike = −5°	Strike = +7.5°	Dip = −2.5°	Dip = +10°	MinSSE	5th Rank Inundation Areas	25th Rank Inundation Areas	45th Rank Inundation Areas
Miyako	[4.12, 2.65]	[3.12, 2.71]	[2.96, 2.56]	[4.38, 3.41]	[2.93, 2.55]	[3.09, 2.65]	[2.99, 2.66]	[4.82, 3.38]	[2.91, 2.49]	[1.04, 1.02]	[2.52, 2.31]	[6.46, 3.24]
Kamaishi	[5.42, 3.42]	[6.91, 2.89]	[6.01, 2.98]	[10.18, 2.78]	[6.46, 2.57]	[6.13, 2.71]	[6.87, 2.88]	[11.36, 2.83]	[5.31, 2.66]	[1.55, 1.54]	[3.94, 2.45]	[10.05, 3.16]
Ofunato	[7.69, 4.92]	[4.93, 3.29]	[3.63, 2.16]	[6.64, 4.95]	[4.53, 3.37]	[4.12, 2.38]	[4.92, 3.50]	[8.07, 4.18]	[5.51, 3.27]	[1.64, 1.26]	[4.96, 4.20]	[6.74, 5.02]
Rikuzentakata	[8.16, 4.58]	[7.77, 5.19]	[6.57, 4.86]	[9.81, 5.83]	[7.36, 5.32]	[5.85, 4.41]	[7.89, 5.30]	[12.70, 6.17]	[7.65, 5.12]	[2.74, 2.68]	[5.63, 4.58]	[8.76, 6.01]
Kesennuma	[4.35, 3.01]	[2.88, 2.12]	[2.42, 1.90]	[3.33, 2.47]	[2.43, 2.00]	[2.96, 2.07]	[2.70, 2.15]	[5.35, 2.80]	[4.19, 2.55]	[1.41, 1.49]	[2.42, 2.22]	[3.53, 2.70]
Onagawa	[7.74, 4.10]	[7.37, 3.87]	[4.27, 3.57]	[12.01, 5.00]	[9.24, 3.88]	[4.12, 3.33]	[9.29, 3.87]	[18.43, 4.99]	[8.24, 4.03]	[1.51, 2.21]	[4.66, 3.75]	[10.05, 5.11]
Ishinomaki	[2.49, 1.99]	[3.20, 2.02]	[2.48, 1.76]	[4.21, 2.29]	[2.59, 1.81]	[1.95, 1.73]	[3.55, 2.13]	[6.03, 2.58]	[2.41, 1.76]	[0.88, 1.38]	[2.81, 1.95]	[3.65, 2.04]
Shiogama	[3.58, 2.93]	[3.65, 2.69]	[3.21, 2.55]	[4.78, 3.74]	[3.10, 2.65]	[2.80, 2.37]	[3.98, 3.01]	[6.61, 4.09]	[2.24, 2.91]	[1.83, 2.50]	[3.84, 3.38]	[4.55, 3.50]
Natori	[2.71, 2.07]	[3.28, 1.59]	[2.62, 1.57]	[4.83, 1.88]	[2.90, 1.56]	[2.14, 1.60]	[3.64, 1.66]	[6.43, 1.95]	[2.53, 1.60]	[1.48, 1.49]	[3.86, 1.80]	[4.83, 1.79]
Yamamoto	[3.75, 2.79]	[2.06, 1.51]	[1.50, 1.35]	[4.08, 2.02]	[2.36, 1.62]	[0.86, 1.27]	[2.57, 1.63]	[6.21, 2.16]	[4.08, 1.99]	[0.57, 1.11]	[3.02, 1.73]	[5.03, 2.18]

study include the inundation areas with depths exceeding threshold values of 1, 2, 3, 5, 7.5, and 10 m. The inundation areas are directly associated with tsunami impact, and are useful for ranking the tsunami simulation results due to variable slip distributions with regards to the extent of the inundation (note: it is not straightforward to order stochastic slip models according to the slip parameters). In addition, Aida's K and κ factors are evaluated for all simulation cases. When evaluating the performance measures of the simulation results, small hazard values could produce unrealistically large values of the performance metrics (although they are of less importance from a tsunami risk viewpoint). For example, in calculating the K and κ factors, the ratio between the observed and simulated depths is computed; this ratio can be extremely large when the simulated inundation depth is very close to zero (and thus they have dominant influence on the calculated performance metrics). Based on the above considerations, TTJS data with inundation depths shallower than 0.5 m are not used for calculating the summary statistics (e.g., SSE). Furthermore, in computing the K and κ factors, simulated inundation depths that are shallower than 0.5 m are excluded.

3.2. Kamaishi in Iwate Prefecture

Kamaishi is situated in an East-facing bay, with urban development concentrated along the Katsushi River. It is bounded by steep hills to North and South. The port of Kamaishi was protected by the deepest breakwaters in the world (the foundation at a depth of 63 m and the freeboard at a height of 6 m above the sea surface), whose construction was completed in 2009. Although the Kamaishi breakwaters were severely damaged during the 2011 Tohoku tsunami, it has been confirmed that the breakwaters were effective in reducing the tsunami waves and delaying the arrival of major waves at the urban areas of Kamaishi [*Mori et al.*, 2013, 2015]. Nonetheless, the tsunami damage and fatalities in Kamaishi were devastating [*Fraser et al.*, 2013].

Figure 3a compares the simulated inundation depth contours based on the original Satake et al. model with the TTJS data. In the coastal defense data that are implemented for tsunami simulation, the Kamaishi breakwaters are represented partially; the northern section of the Kamaishi breakwaters exists, whereas about 30% of the southern section of the Kamaishi breakwaters is present in the coastal defense data. Hence, it is expected that the simulation result for the base case overestimates the inundation extent to some degree. The color scheme for the contours is: blue for 0 m depth and red for 10 m depth. The TTJS results are displayed as circles filled with different colors (see the figure legend). The color coding for the TTJS data is similar to the color range adopted for the tsunami simulation contours. This facilitates the visual inspection and comparison of the simulated inundation depth contours with the TTJS results. In addition, scatter plot and histograms of the observed and simulated inundation depth data are shown (Figures 3b and 3c, respectively). Figure 3 indicates that the simulated footprints are more severe than the TTJS data; the mean inundation depths for the simulated and observed data are 6.91 and 5.42 m, respectively. Consequently, the K factor for the original Satake et al. model is less than 1.0 (=0.71). The linear correlation between the simulation and the observations is 0.69. The overprediction of the simulated inundation depths can be seen in the scatter plot and histograms (Figures 3b and 3c), however, interestingly the spatial extent of inundation for the simulation is similar to that for the observations.

Moreover, Figure 3 includes the results based on the slip model achieving the MinSSE with respect to the survey data out of 50 stochastically generated slip distributions (i.e., best matching result with the observations among the variable slip cases). Because the best matching slip models are obtained for individual cities (i.e., the error statistics are defined locally), the shown cases for different cities and towns, are not

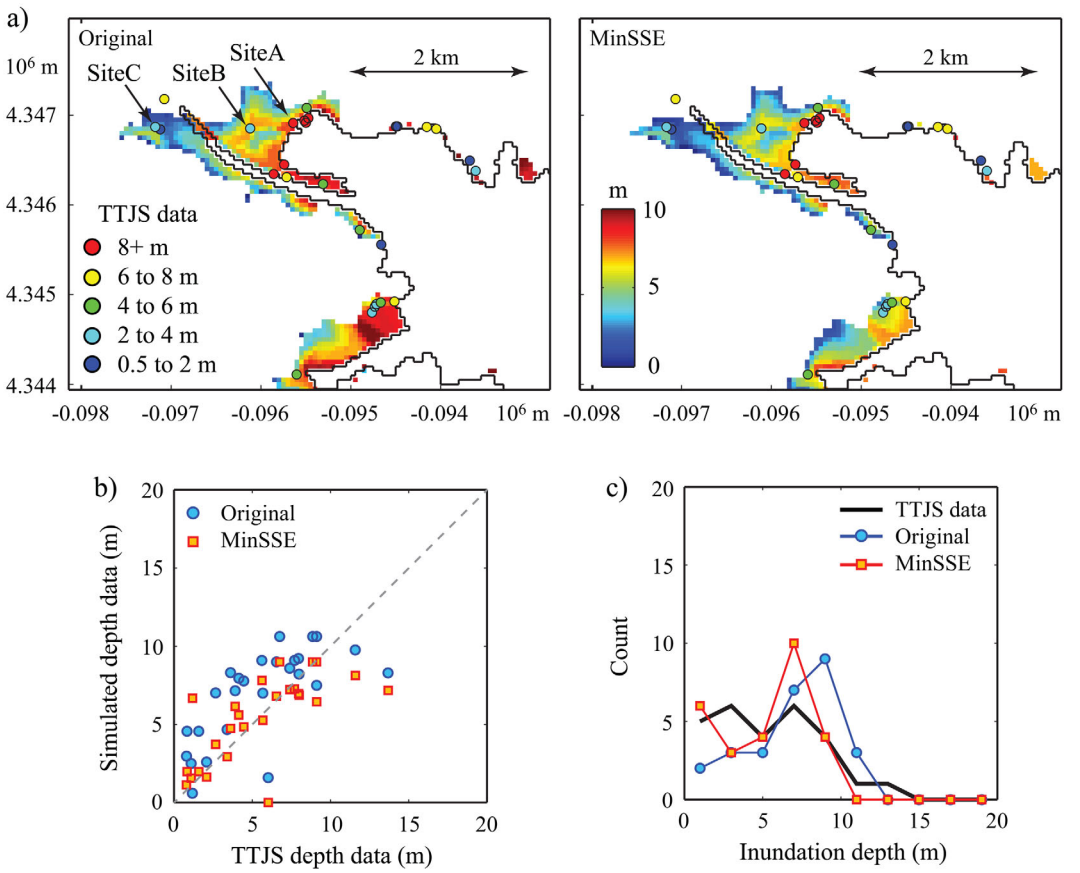

Figure 3. Tsunami simulation results for Kamaishi: (a) inundation depth contours, (b) scatter plot, and (c) histograms based on the Satake et al. model and the minimum SSE slip distribution.

identical. The MinSSE case is less severe than the original case and achieves closer agreement with the TTJS data (e.g., mean inundation depth is 5.31 m and the linear correlation is 0.71; see Table 1).

Before discussing tsunami inundation footprints in Kamaishi (which are spatially aggregated tsunami hazard parameters), it is instructive to examine the variability of tsunami inundation depths at specific locations due to the slip variations (i.e., 50 cases). For this purpose, the conditional cumulative probability distribution functions of the tsunami inundation depths at three TTJS sites are compared in Figure 4. The term *conditional* is included to specify that the tsunami hazard assessments are conducted by referring to a particular scenario (i.e., events similar to the 2011 Tohoku earthquake), rather than all possible events in the Tohoku region. The locations of the selected TTJS sites are shown in Figure 3a. In the Figure 4 legend, the elevations as well as the statistics, i.e., mean and coefficient of variation (CoV), of inundation depth for the three sites are indicated. Additionally, the TTJS observations at the three locations are represented by a star in the figure. For Kamaishi, site A is near the coastline, site B is located in the center of the urban areas, and site C is at further inland (note: the elevations for sites A, B, and C gradually increase; see Figure 3a). As expected, the probability distribution functions of the inundation depth gradually shift toward left as the elevation of the TTJS sites becomes higher (this can be inspected by their mean inundation depths). The CoV of the inundation depth tends to become larger as the elevation of the TTJS sites becomes higher. This is because when tsunami sources are distant from Kamaishi (e.g., major asperities are located in the southern/central part of the Tohoku region), inland sites are not inundated, while if tsunami sources are close to Kamaishi then massive tsunami waves can inundate the majority of the low-lying part of the city (see Figure 6).

The sensitivity results for variable geometrical parameters are compared in Figure 5, showing simulated inundation depth contours based on the top-edge depth variations of −2.5 km and +10 km, strike variations of −5° and +7.5°, and dip variations of −2.5° and +10° with respect to the reference model (for each parameter, the minimum and maximum cases are presented; see Table 1 for the inundation depth statistics). The contours

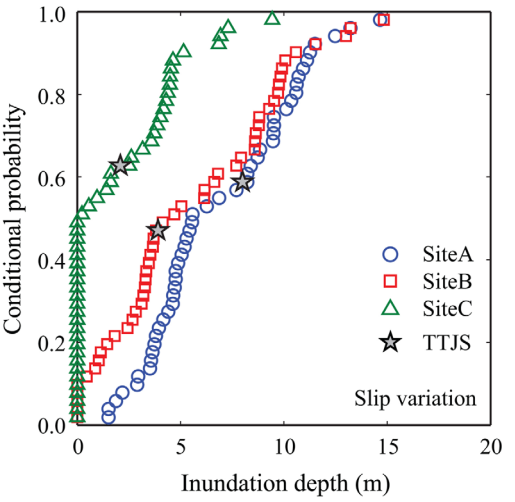

Figure 4. Variability of inundation depths at sites A, B, and C in Kamaishi due to the slip variations. See Figure 3a for the locations on the map.

facilitate the visual examination of the ranges of simulation results for different geometrical parameters. The top-edge depth and dip variations have major influence on the inundation footprints, whereas the effects due to the strike variations are negligible.

Figure 6 shows the simulated inundation depth contours based on the slip models that are associated with the 5th, 25th, and 45th inundation areas above 1 m depth out of 50 stochastically generated slip distributions. The contours visualize the variability of the inundation footprints due to the slip variations (i.e., stochastic inundation maps). The inundation depths and areas can vary significantly, depending on the slip distributions; the areas vary from 0.5 to 2.4 km^2 and the maximum depth increases from about 3 m to more than 10 m.

Next, the sensitivity and variability of inundation extent and K and κ metrics are investigated quantitatively for all 66 cases. Figures 7a–7c show the sensitivity of inundation areas with different depth thresholds (i.e., above 1, 2, 3, 5, 7.5, or 10 m depth) to the top-edge depth, strike, and dip, respectively. This analysis illustrates the sensitivity to the top-edge depth, strike, and dip variations based on the inundation areas with different depth thresholds (note: similar plots for the K and κ factors are produced but not presented for brevity; the K factor decreases slightly with the increasing depth and dip variations, whereas the κ factor remains stable and fluctuates around 1.8). Figures 7a–7c indicate that the inundation areas above 1 m depth only increase gradually as a function of the top-edge depth or dip angle, while the areas above 10 m depth tend to increase more rapidly as these parameters increase. This is because for the original case, most of the low-lying areas in Kamaishi are already inundated and such low-elevation areas are bounded by the steep hills. A small increase of tsunami wave heights results in much greater inundation areas when the local topography is relatively flat. On the other hand, the tsunami inundation for topography with steep slopes is not much affected by a small increase of the tsunami wave heights. In short, the changes of the inundation areas are nonlinear in terms of depth threshold, and strongly depend on the local topographical characteristics.

Figure 7d shows the conditional cumulative probability distribution for slip variations based on the inundation areas with different depth thresholds; Figure 7e displays similar variability results for the K and κ factors. These plots visualize the possible ranges of the adopted tsunami hazard metrics. The results shown in Figure 7d indicate that the upper bound of the inundation areas in Kamaishi is about 2.5 km^2. When more extensive slip distributions are considered, the inundation areas above shallower depths (less than 5 m) do not increase significantly, whereas those above deeper threshold values (greater than 5 m) increase rapidly. The K factor changes widely from 0.3 to 2.7 due to the slip variations, while the κ factor is more stable with respect to the alternative slip models (Figure 7e). The K factor plot can be used to examine the level corresponding to the observed data in terms of the stochastically generated scenarios. For instance, a K factor of 1.0 approximately corresponds to the conditional probability level of 0.5, indicating that the 2011 Tohoku inundation may not be the worst-case scenario for Kamaishi (judged based on a single reference model only). Finally, the comparison of the results shown in Figures 7a–7d suggests that the slip variations have more significant influence than the top-edge depth/strike/dip variations, and thus it is essential to consider alternative slip scenarios in exploring the possible range of tsunami inundation footprints.

3.3. Onagawa in Miyagi Prefecture

Onagawa is situated in a narrow valley exposed to the ocean in the East-facing direction. Because of its location and topography, very large tsunami waves were generated by the 2011 Tohoku earthquake. In

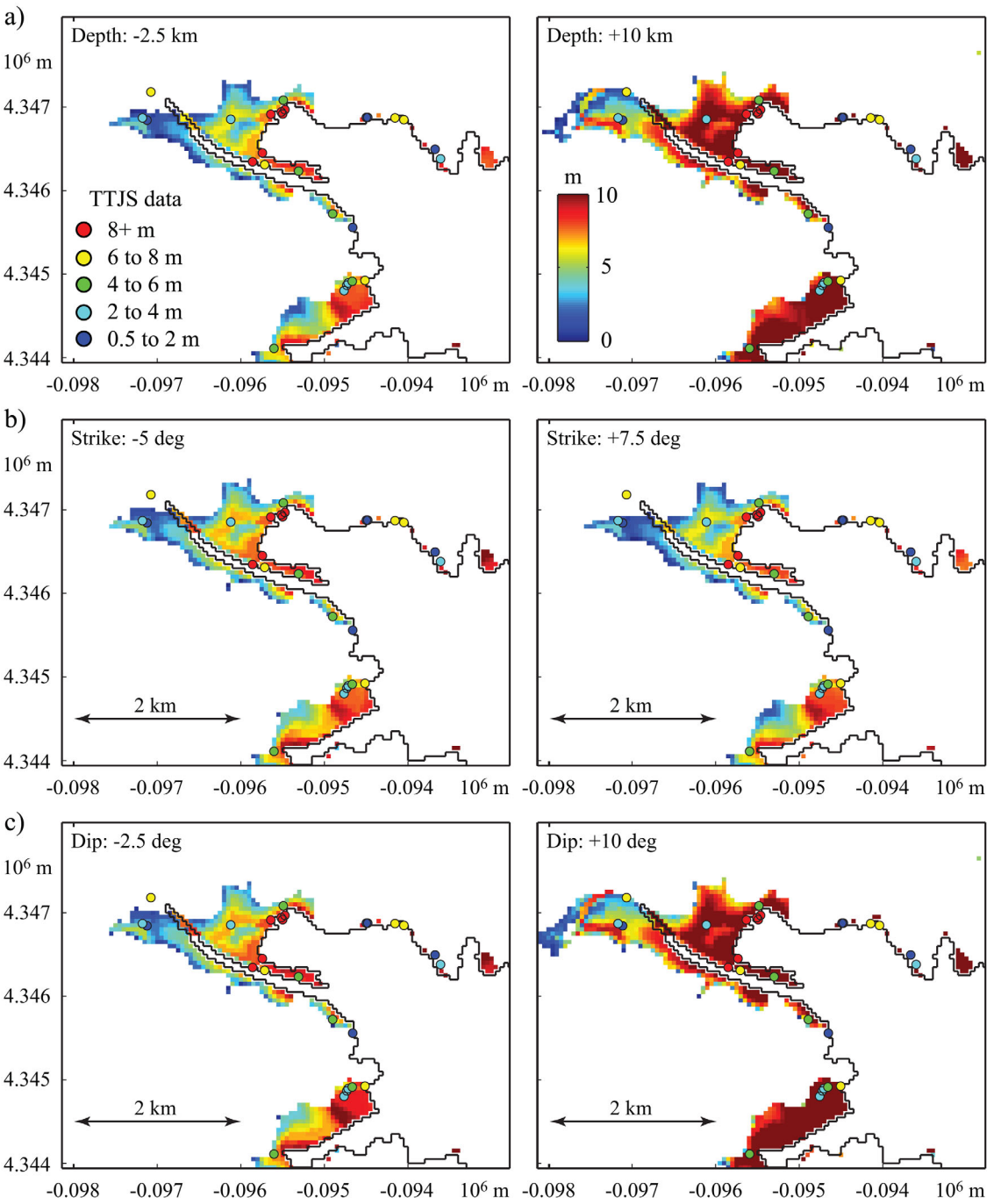

Figure 5. Sensitivity of inundation depth contours for Kamaishi: (a) top-edge depths of −2.5 km and +10 km, (b) strike angles of −5° and +7.5°, and (c) dip angles of −2.5° and +10°.

particular, the majority of buildings in low-lying areas were completely inundated and destroyed; the maximum inundation depths exceeded 16 m. In addition to the direct tsunami effects, a large subsidence of 1.2 m was observed in Onagawa due to coseismic deformation of the 2011 Tohoku earthquake. Because of the very large tsunami waves arriving within a relatively short time after the earthquake (about 30 min), the fatality rate among the population residing in the inundated areas was particularly high in Onagawa [*Fraser et al.*, 2013].

The same set of tsunami simulation results that are considered for Kamaishi (i.e., Figures 3–7) is presented in Figures 8–12 for Onagawa. The inundated areas based on the Satake et al. model are in good agreement with

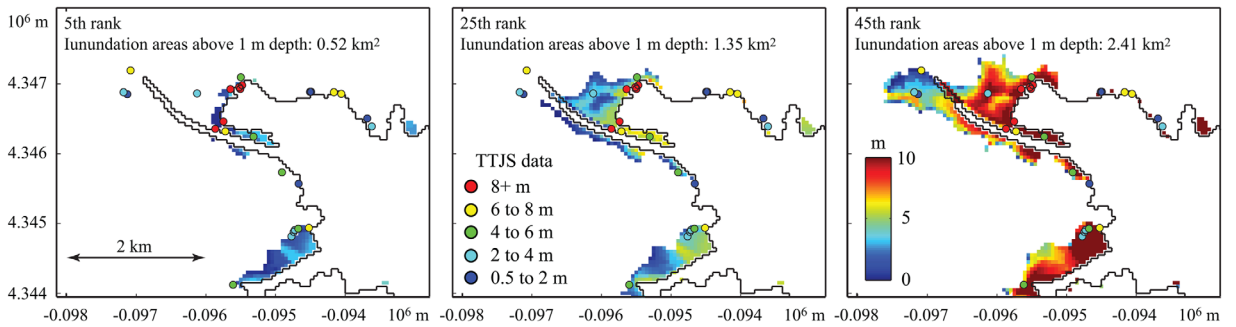

Figure 6. Inundation depth contours for Kamaishi: 5th rank, 25th rank, and 45th rank based on the inundation areas above 1 m depth out of 50 stochastic slip cases.

the observed inundation data (Figure 8a). The very deep inundation at the low-lying parts of Onagawa can be observed clearly. Although the number of the TTJS data points is relatively small, the scatter plot and histograms of the simulated and observed data show good agreement (e.g., mean inundation depths of 7.37 versus 7.74 m; K factor = 0.98; Figures 8b and 8c). The linear correlation coefficient is 0.81. Furthermore, the inundation depth contours for the MinSSE case is similar to (but slightly more severe than) the original case.

Figure 9 compares the conditional cumulative probability distribution functions of inundation depths at three TTJS locations (see Figure 8a) in Onagawa due to the slip variations. The results show that the variability of tsunami inundation depths at specific sites can be large. The average inundation depth decreases with the distance from the coastline (i.e., elevation of the sites increases), whereas the CoV of inundation depth increases.

The sensitivity analysis for the geometrical parameters shows that all three parameters have significant influence on the tsunami inundation (Figure 10). Inundation depth increases with the top-edge depth and dip variations, while it decreases with the strike variations (Figures 12a–12c). The strong sensitivity to the fault strike is attributed to the fact that Onagawa directly faces major earthquake rupture areas of the 2011

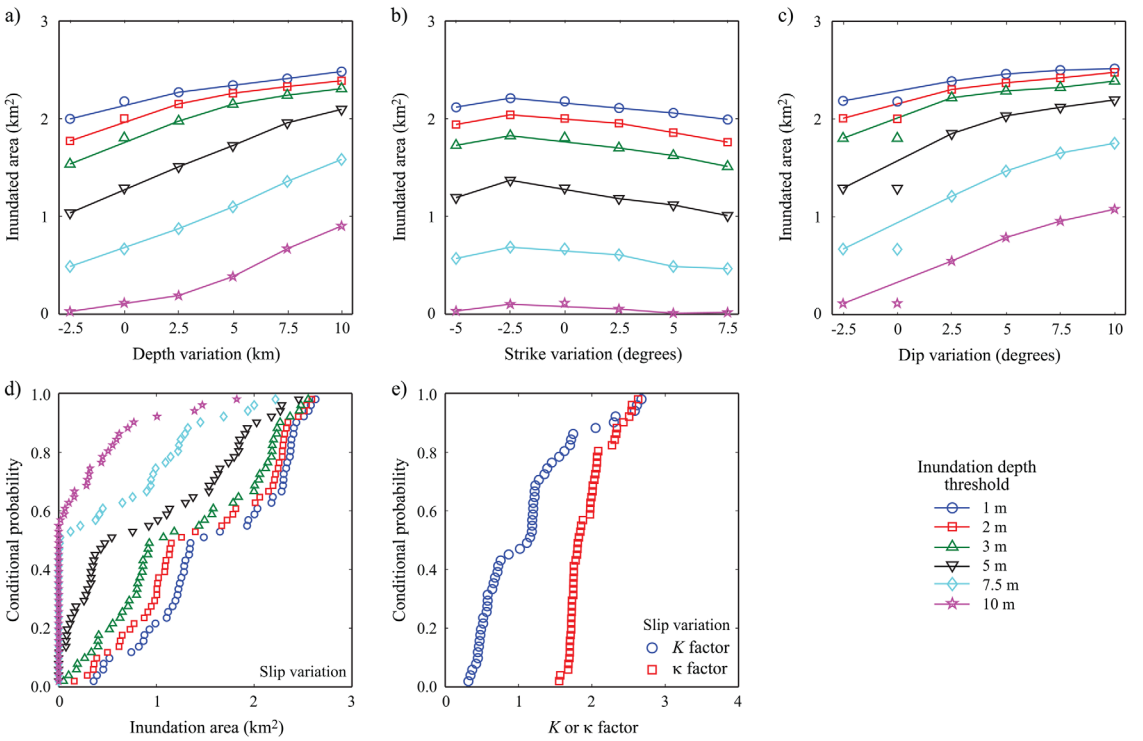

Figure 7. Sensitivity analysis results for Kamaishi: sensitivity of inundation areas to the (a) top-edge depth variations, (b) strike variations, (c) dip variations, (d) variability of inundation areas, and (e) K and κ factors due to the slip variations.

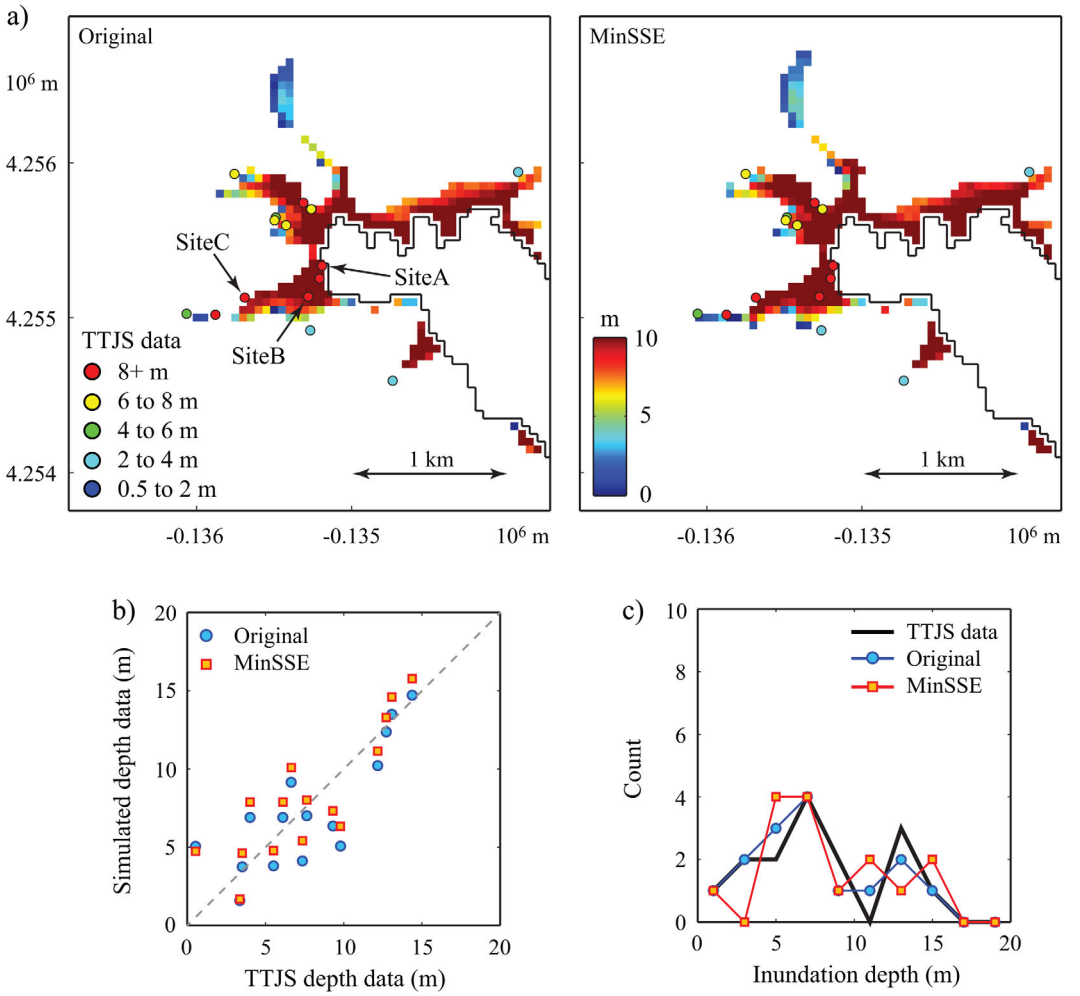

Figure 8. Tsunami simulation results for Onagawa: (a) inundation depth contours, (b) scatter plot, and (c) histograms based on the Satake et al. model and the minimum SSE slip distribution.

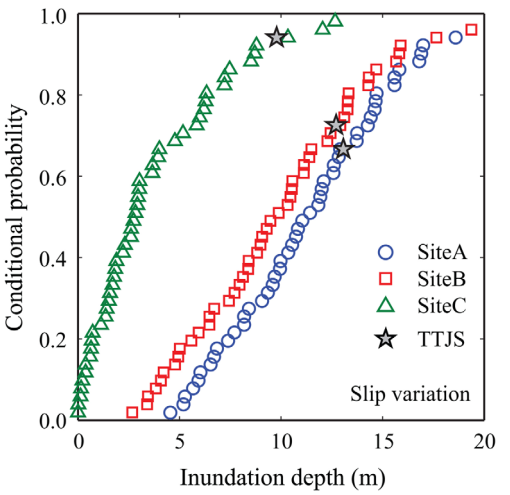

SiteA
Elevation: 1.47 m
Mean: 11.43 m
CoV: 0.353

SiteB
Elevation: 3.43 m
Mean: 9.93 m
CoV: 0.432

SiteC
Elevation: 10.91 m
Mean: 3.69 m
CoV: 0.880

Figure 9. Variability of inundation depths at sites A, B, and C in Onagawa due to the slip variations. See Figure 8a for the locations on the map.

Tohoku earthquake (see Figure 2). The high sensitivity to the geometrical parameters is also observed for the K factor, while the κ factor slightly varies with the top-edge depth and strike variations, but remains almost constant for the dip variations (note: results are omitted for brevity).

The ranked inundation footprints based on the inundation areas above 1 m depth (Figure 11) suggest that the spatial extent of the inundated areas changes from the 5th rank case to the 25th rank case. On the other hand, from the 25th rank case to the 45th rank case, major changes

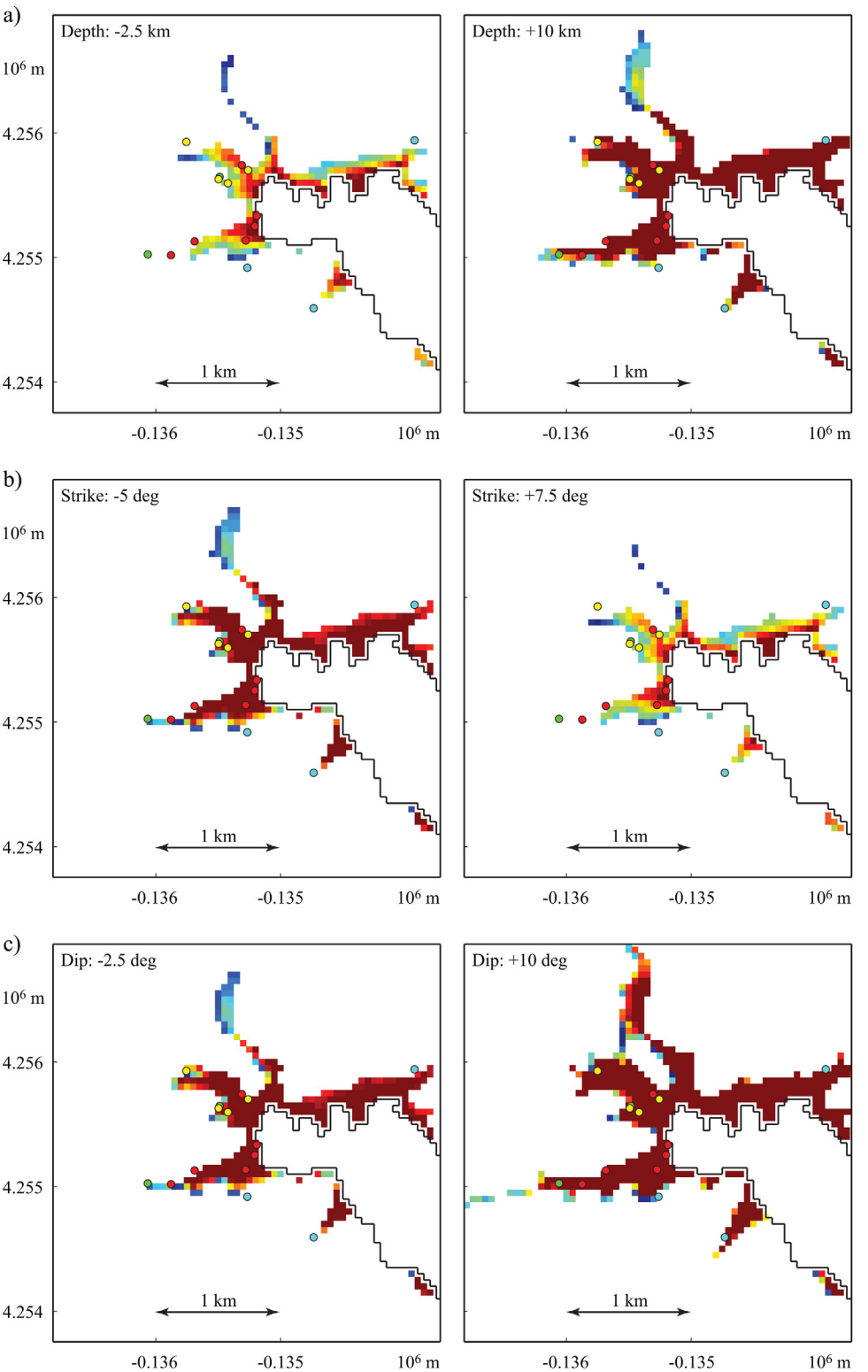

Figure 10. Sensitivity of inundation depth contours for Onagawa: (a) top-edge depths of −2.5 km and +10 km, (b) strike angles of −5° and +7.5°, and (c) dip angles of −2.5° and +10°.

occur mostly to inundation depths, rather than inundation areas. Such trends can also be seen in Figure 12d; the inundation areas for all depth thresholds are practically bounded at 1 km^2. Figure 12e shows that the *K* factor varies very widely (from 0.5 to 5.0) due to the slip variations, indicating that the tsunami inundation in

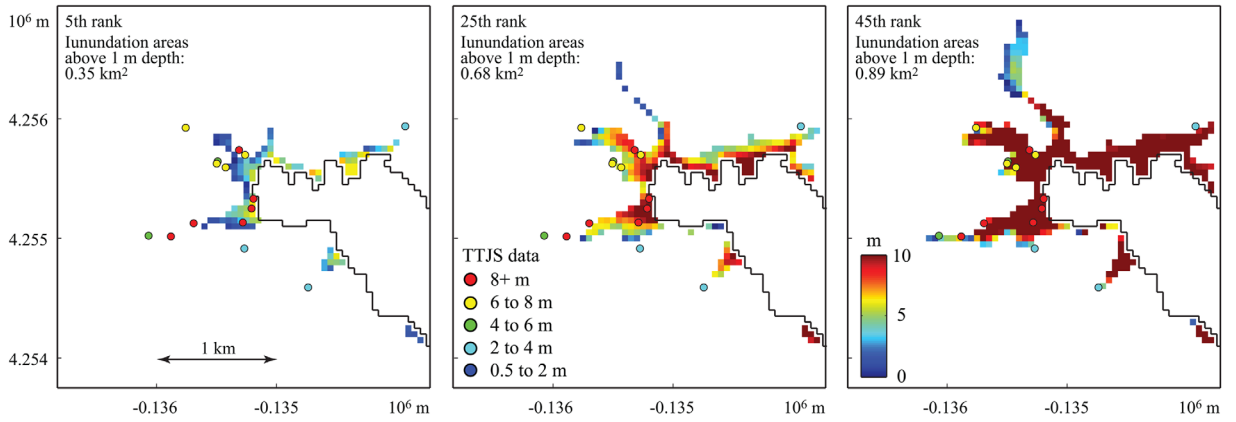

Figure 11. Inundation depth contours for Onagawa: 5th rank, 25th rank, and 45th rank based on the inundation areas above 1 m depth out of 50 stochastic slip cases.

Onagawa is very sensitive to slip characteristics. The conditional probability level corresponding to the *K* factor of 1.0 is 0.2; thus the observed tsunami during the 2011 Tohoku event may be considered as one of the worst-case scenarios for this town.

3.4. Sendai-Natori-Iwanuma in Miyagi Prefecture

Sendai, Natori, and Iwanuma are positioned in the Sendai plain (note: the Sendai airport is in Iwanuma). They are the most populated areas in Miyagi Prefecture. Two major rivers, the Natori River and the Abukuma River, run through the areas. The flat terrain contributed significantly to extensive inundation areas during the 2011 Tohoku tsunami. The inundation reached the Sendai Tobu Highway, which runs South-North at about 2–5 km from the coast. The 10 m embankment of the highway reduced the tsunami inundation significantly [*Goto et al.*, 2012]. The destruction of residential districts near the shoreline (e.g., Arahama and Yuriage) was particularly severe. Because of the unexpectedly

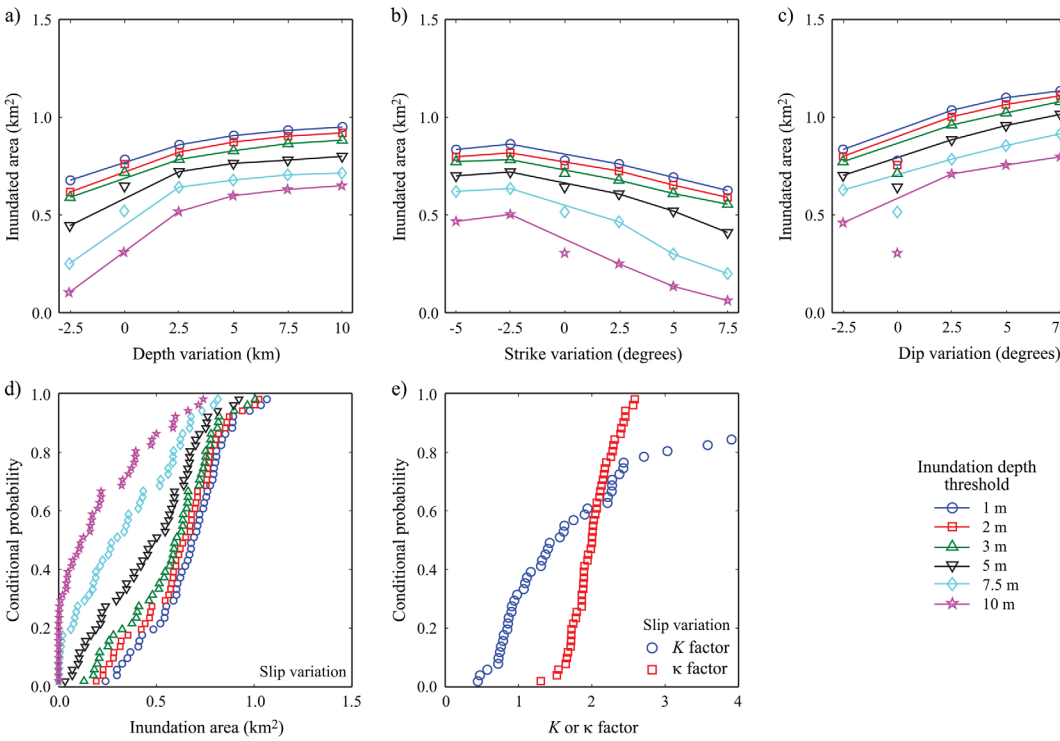

Figure 12. Sensitivity analysis results for Onagawa: sensitivity of inundation areas to the (a) top-edge depth variations, (b) strike variations, (c) dip variations, (d) variability of inundation areas, and (e) *K* and κ factors due to the slip variations.

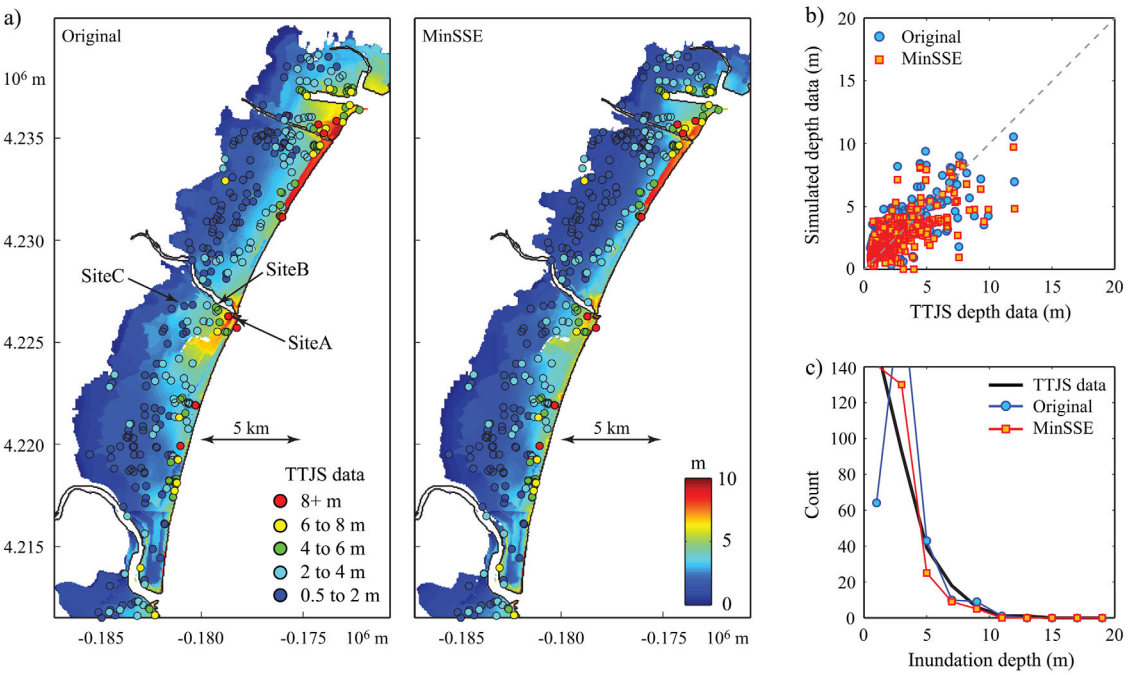

Figure 13. Tsunami simulation results for Sendai-Natori-Iwanuma: (a) inundation depth contours, (b) scatter plot, and (c) histograms based on the Satake et al. model and the minimum SSE slip distribution.

large tsunami, the fatality rates in the severely inundated areas were relatively high [*Fraser et al.*, 2013].

The same set of tsunami simulation results that are considered for Kamaishi (i.e., Figures 3–7) is presented in Figures 13–17 for Sendai-Natori-Iwanuma. Figure 13 compares the inundated areas based on the Satake et al. model and the TTJS data. Generally, the simulated and observed data are in agreement; the mean inundation depths of the simulated and observed data are 3.28 and 2.71 m, respectively (K factor = 0.70), and the linear correlation coefficient is 0.69. In the tsunami simulations, the embankment of the highway is not represented in the DEM, and thus the spatial extent of the simulated inundation to further inland may be overestimated. Another notable feature of the tsunami inundation contours in Sendai is the narrow strip of land that has particularly large inundation depths along the shoreline. This corresponds to a segment of Teizan Canal, which connects Shiogama and Iwanuma. Moreover, the inundation depth contours for the MinSSE case are similar, but slightly more severe than the original case.

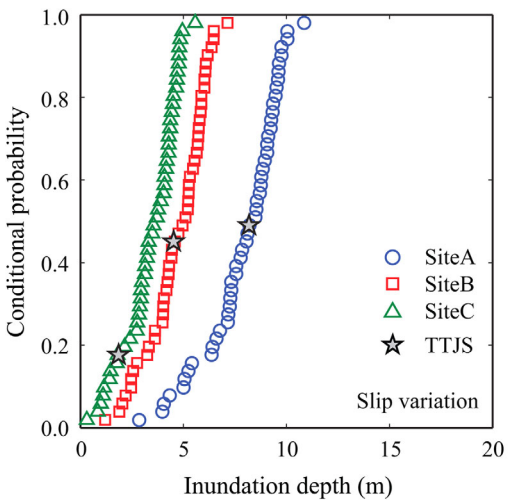

Figure 14. Variability of inundation depths at sites A, B, and C in Sendai-Natori-Iwanuma due to the slip variations. See Figure 13a for the locations on the map.

Figure 15 shows the variability of inundation depths at three TTJS locations in Natori due to the slip variations. Because of the flat terrain in Sendai plain, the elevations of the three TTJS sites are similar but the distances from the shoreline are different (Figure 14a). The conditional cumulative probability distribution plots of the inundation depths at the three locations clearly show that the average inundation depth decreases with the distance from

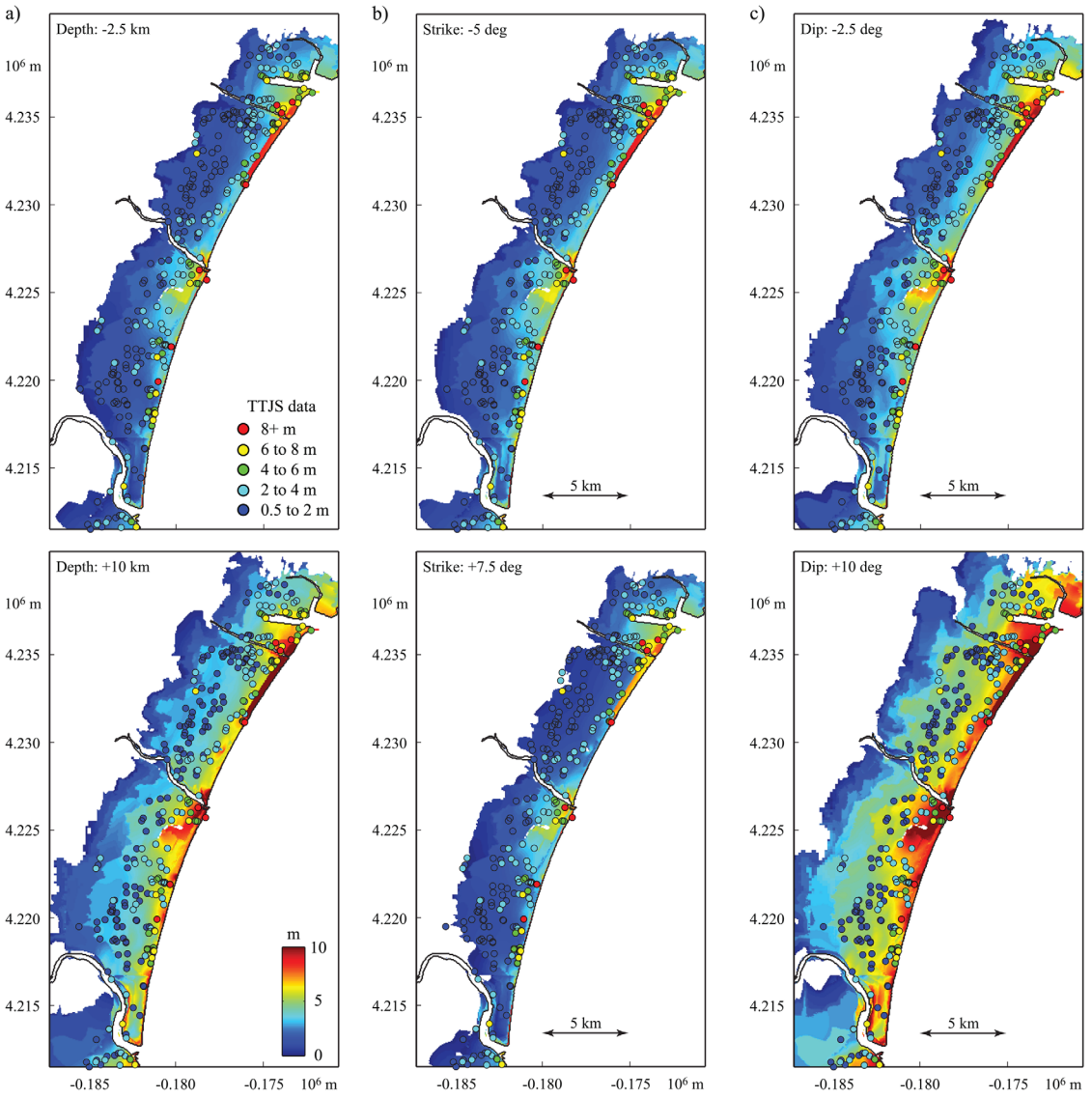

Figure 15. Sensitivity of inundation depth contours for Sendai-Natori-Iwanuma: (a) top-edge depths of −2.5 km and +10 km, (b) strike angles of −5° and +7.5°, and (c) dip angles of −2.5° and +10°.

the shoreline. This is due to the bottom friction. Further to note, the CoV values for the TTJS sites in Natori are significantly smaller than those in Kamaishi and Onagawa. The result is influenced by the location and extent of major asperities and the topographical features [see also *Goda et al.*, 2014].

The sensitivity analysis for the geometrical parameters (Figure 15) indicates that the top-edge depth and dip parameters have major influence on the tsunami inundation, while the effects due to the strike variations are less pronounced. The inundation areas for shallow and deep depth thresholds exhibit different tendencies (Figures 17a–17c). The inundation areas for depths less than 5 m are affected by variations of geometrical parameters. On the other hand, the inundation areas for depth greater than 5 m are less sensitive to such changes. These trends are due to the flat terrain of this region. Variations in geometrical parameters have only moderate influence on the *K* factor.

The ranked inundation footprints based on the inundation areas above 1 m depth (Figure 16) suggest that both spatial inundation extent and inundation depth increase as the considered scenario becomes more extreme. For the worst-case scenario, the inundation areas above 1 m depth reach a topographical boundary where the elevations start to become steeper. This tendency can be seen in the conditional cumulative probability distribution function plot of the inundation depths (Figure 17d); the curve for the 1 m depth threshold

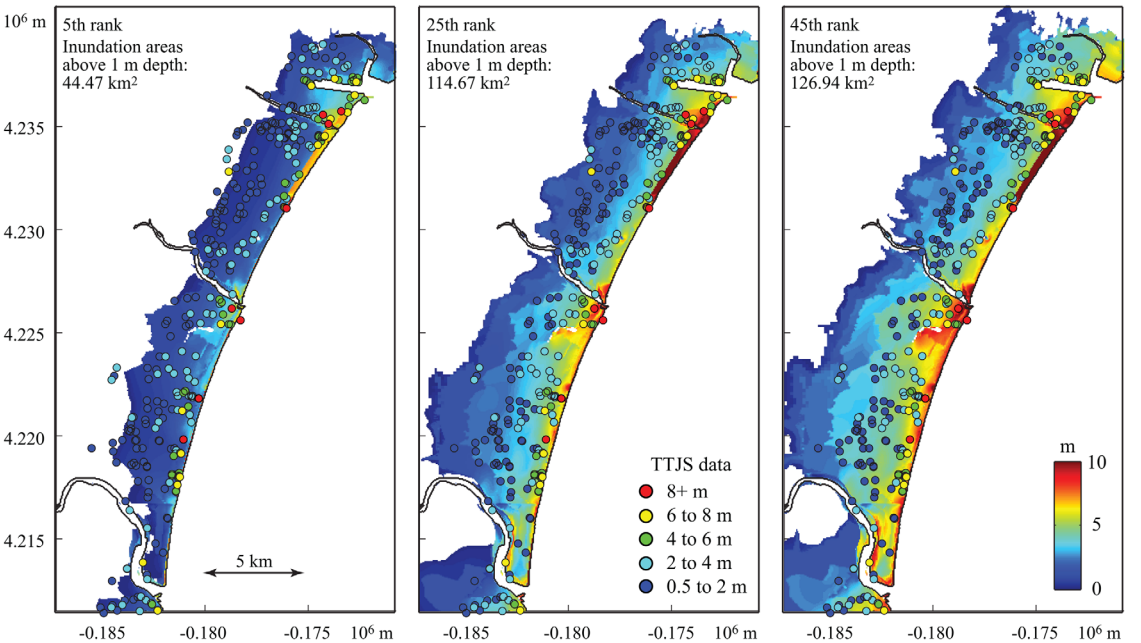

Figure 16. Inundation depth contours for Sendai-Natori-Iwanuma: 5th rank, 25th rank, and 45th rank based on the inundation areas above 1 m depth out of 50 stochastic slip cases.

initially increases gradually, but the slope of the curve becomes steeper (nearly vertical) as the conditional probability level increases. The *K* factor for slip variations (Figure 17e) exhibits a unique feature; for the majority of the slip cases (up to the conditional probability level of 0.8), the *K* factor varies within a narrow range between 0.4 and 1.0, while only a small subset of the cases has the *K* factor greater than 1.0. This indicates

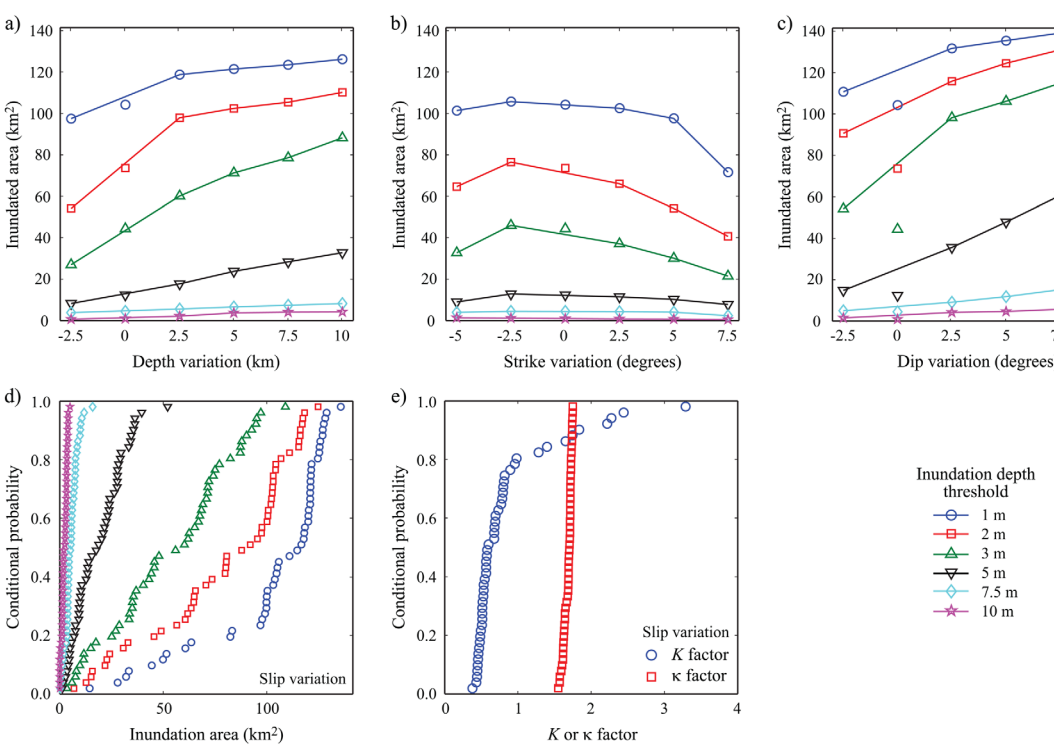

Figure 17. Sensitivity analysis results for Sendai-Natori-Iwanuma: sensitivity of inundation areas to the (a) top-edge depth variations, (b) strike variations, and (c) dip variations, and (d) variability of inundation areas and (e) *K* and κ factors due to the slip variations.

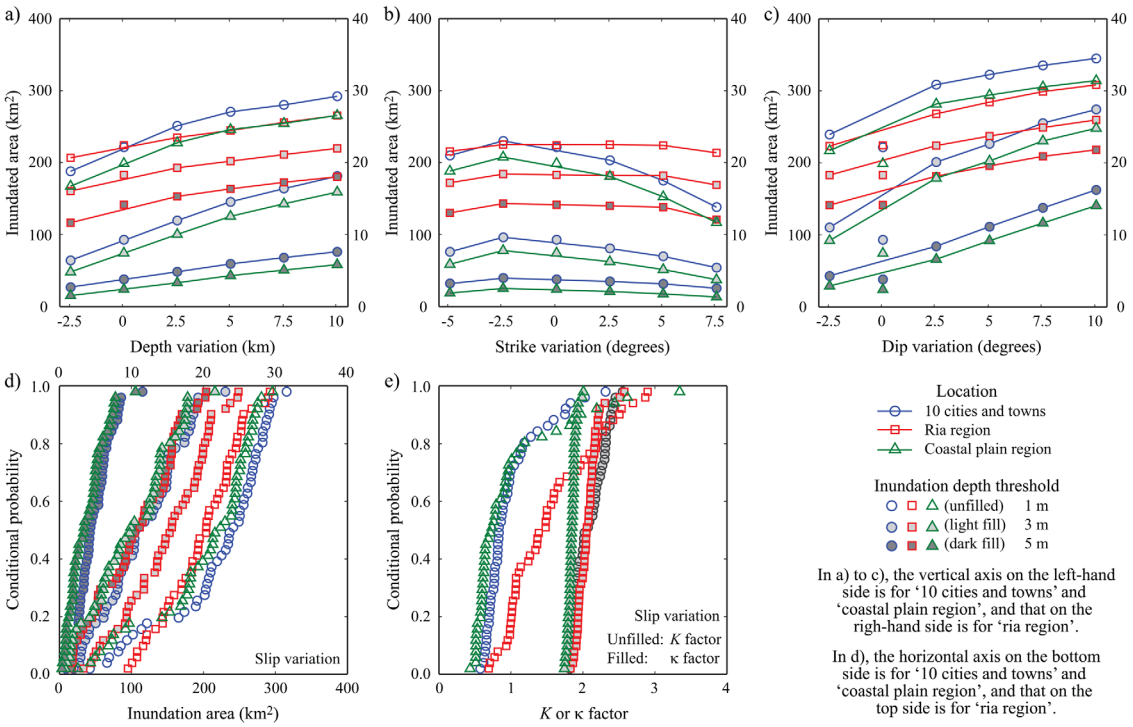

Figure 18. Sensitivity analysis results for 10 cities and towns, ria regions, and coastal plain regions: sensitivity of inundation areas to the (a) top-edge depth variations, (b) strike variations, and (c) dip variations, and (d) variability of inundation areas and K and κ factors (e) due to the slip variations. For Figures 18a–18d, results for the inundation depth thresholds of 1, 3, and 5 m only are presented.

that the chance of experiencing a similar tsunami inundation extent as for the 2011 Tohoku earthquake may be considered likely in a future M_w9 subduction earthquake in the Tohoku region.

3.5. Combined Results for 10 Cities and Towns in the Tohoku Region

The similarity between the simulated inundation depths based on the original Satake et al. model and the observations depends on the location, affected by the assumed tsunami source characteristics, and local topography. For instance, the simulated inundation depths in Ofunato underpredict the TTJS data; for relatively shallow depths inundation data are generally well reproduced, while a large discrepancy is observed for several survey locations along the coastline where large depths are observed. It is important to recognize that the inundation depths at these coastal locations may be inaccurate due to inundation height-to-depth adjustment. On the other hand, in Watari-Yamamoto-Soma, more consistent differences between the simulation and the observations are seen in the southern part of the areas. Such differences may be attributed to the earthquake source characteristics (e.g., local slip patch in the southern part of the fault plane and the strike angle). The systematic assessment of the sensitivity of the tsunami simulation results to fault geometry and slip distribution provides valuable insights into the complex inundation processes.

The sensitivity and variability results for the combined region of 10 cities and towns (blue lines) are shown in Figure 18. Moreover, two additional regions, ria and coastal plain, are defined and the results for these cases are included in Figure 18 (red and green lines for the ria and coastal plain regions, respectively). In Figures 18a–18d, different scales for the inundation areas are adopted for the combined and coastal plain regions and for the ria region. For brevity, inundation depth thresholds of 1, 3, and 5 m are considered. The sensitivity of inundation areas of the combined region above different depth thresholds to the geometrical parameters shows increasing, decreasing, and increasing trends for the top-edge depth, strike, and dip variations, respectively. The results also exhibit variable sensitivity for different threshold depths. The general features of the sensitivity results for the 10 cities and towns are similar to those for Sendai-Natori-Iwanuma (Figure 17). This is expected because the adopted tsunami hazard parameter is the total inundation areas, relative contributions to which are greater for locations in the Sendai plain (i.e., Ishinomaki to Yamamoto). The differences between the coastal plain region and the ria region are clear (red versus green lines; note the scales for inundation areas are different). Although inundation areas for the ria region are less sensitive

to increase in top-edge depth variation, inundation areas for the coastal plain region increase monotonically as the depth variation increases. The depth variation gives a factor of 2–3 difference for inundation areas in the coastal plain region. The positive strike variation decreases the inundation areas in the coastal plain region, but gives less influence in the ria coast region (at more local levels, the strike variation does affect inundation areas, e.g., Onagawa; see Figure 12b). Generally, the sensitivity of tsunami inundation areas to fault geometry is significant in the coastal plain region. Therefore, it is important to know how sensitive a target region is to fault geometry for expected tsunami scenarios.

It is noteworthy that the impacts of the fault geometry and slip distribution vary spatially along the Tohoku coast (i.e., ria region to coastal plain region), indicating that critical scenarios with similar magnitudes for tsunami hazard mapping and planning should be developed by taking into account such key features.

4. Conclusions

This study investigated the sensitivity and variability of tsunami inundation footprints in 10 coastal cities and towns due to a megathrust subduction earthquake in the Tohoku region of Japan by considering different fault geometry and slip distributions. The variations of earthquake source characteristics were represented with respect to the Satake et al. source model by changing the top-edge depth, strike, dip, and slip distributions. The slip variations were implemented based on the spectral analysis and synthesis method for a M_w9 megathrust subduction earthquake, developed by *Goda et al.* [2014]. For evaluating inundation footprints at submunicipality levels, tsunami simulations were carried out using bathymetry and elevation data with 50 m grid spatial resolution. The investigations facilitated the development of stochastic inundation depth maps and the variability assessment of tsunami hazard estimates. Such information is critical to anticipate the potential consequences under different conditions, and to communicate variability associated with hazard predictions for tsunami risk management purposes.

The main conclusions of this study are:

1. The sensitivity of inundation areas and performance metrics (e.g., K and κ factors) to the geometrical parameters is nontrivial. An increase in top-edge depth results in greater tsunami inundation. In particular, when large slip exists at shallow depth near the Trench, the impact of the depth variations tend to be greater. The effects due to the strike variations can be either constant, increasing, decreasing, or combination of those, and depend on the location of large slip asperities relative to the site location. An increase in dip leads to greater tsunami inundation.
2. The variability of inundation footprints due to variable slip distributions can be significant. Generally speaking, the effects due to the slip variations are more significant than those due to the variable geometrical parameters of the earthquake source. Using stochastically generated earthquake slip models, many realizations of inundation depth maps can be obtained. These are particularly effective in visualizing and communicating uncertainty associated with the tsunami input boundary conditions. These inundation simulations are also useful for evaluating observed (historical) tsunami inundation cases in terms of the possible ranges of the inundation depths and areas for future scenarios.
3. Both the sensitivity and variability assessments of tsunami inundation depths depend strongly on local topography. In ria regions, where cities and towns are surrounded by steep hills, the spatial extent of tsunami inundation is often determined by the abrupt changes of elevation. In such cases, the inundation areas for different depth thresholds are not significantly affected but their depths increase greatly. On the other hand, in coastal plain regions, tsunami inundation areas vary significantly for different tsunami scenarios. Therefore, it is of critical importance to account for nonlinear inundation processes and topographical effects when assessing uncertainty in developing tsunami hazard maps, but also for generating evacuation maps for local communities.

Acknowledgments
The bathymetry and elevation data for the Tohoku region were provided by the Cabinet Office of the Japanese Government. The runup and inundation survey data were obtained from the 2011 Tohoku Earthquake Tsunami Joint Survey Group (http://www.coastal.jp/tsunami2011/). This work was supported by the Engineering and Physical Sciences Research Council (EP/M001067/1) as well as by the King Abdullah University of Science and Technology (KAUST). The authors thank two anonymous reviewers for their insightful comments and suggestions that improved the clarity of the paper significantly.

References

Aida, I. (1978), Reliability of tsunami source model derived from fault parameters, *J. Phys. Earth*, *26*, 57–73.
Bilek, S. L., and T. Lay (1999), Rigidity variations with depth along interpolate mega-thrust faults in subduction zones, *Nature*, *400*, 443–446.
Federal Emergency Management Agency (FEMA) (2008), Guidelines for design of structures for vertical evacuation from tsunamis, *FEMA P646*, Fed. Emergency Manage. Agency, Washington, D. C.

Fraser, S., A. Pomonis, A. Raby, K. Goda, S. C. Chian, J. Macabuag, M. Offord, K. Saito, and P. Sammonds (2013), Tsunami damage to coastal defences and buildings in the March 11th 2011 M_w9.0 Great East Japan earthquake and tsunami, *Bull. Earthquake Eng.*, *11*, 205–239.
Fujii, Y., K. Satake, S. Sakai, S. Shinohara, and T. Kanazawa (2011), Tsunami source of the 2011 off the Pacific coast of Tohoku earthquake, *Earth Planets Space*, *63*, 815–820.
Geist, E. L. (2002), Complex earthquake rupture and local tsunamis, *J. Geophys. Res.*, *107*(B5), 2086, doi:10.1029/2000JB000139.
Geist, E. L., and S. L. Bilek (2001), Effect of depth-dependent shear modulus on tsunami generation along subduction zones, *Geophys. Res. Lett.*, *28*, 1315–1318, doi:10.1029/2000GL012385.
Geist, E. L., and T. Parsons (2006), Probabilistic analysis of tsunami hazards, *Nat. Hazards*, *37*, 277–314.
Glimsdal, S., G. K. Pedersen, C. B. Harbitz, and F. Løvholt (2013), Dispersion of tsunamis: Does it really matter?, *Nat. Hazards Earth Syst. Sci.*, *13*, 1507–1526.
Goda, K., P. M. Mai, T. Yasuda, and N. Mori (2014), Sensitivity of tsunami wave profiles and inundation simulations to earthquake slip and fault geometry for the 2011 Tohoku earthquake, *Earth Planets Space*, *66*, 105, doi:10.1186/1880–5981-66–105.
Goto, C., Y. Ogawa, N. Shuto, and F. Imamura (1997), Numerical method of tsunami simulation with the leap-frog scheme (IUGG/IOC Time Project), *IOC Manual 35*, The United Nations Educational, Scientific and Cultural Organization, (UNESCO) Paris.
Goto, K., K. Fujima, D. Sugawara, S. Fujino, K. Imai, R. Tsudaka, T. Abe, and T. Haraguchi (2012), Field measurements and numerical modeling for the run-up heights and inundation distances of the 2011 Tohoku-oki tsunami at Sendai Plain, Japan, *Earth Planets Space*, *64*, 1247–1257.
Gusman, A. R., Y. Tanioka, S. Sakai, and H. Tsushima (2012), Source model of the great 2011 Tohoku earthquake estimated from tsunami waveforms and crustal deformation data, *Earth Planet. Sci. Lett.*, *341–344*, 234–242.
Hooper, A., J. Pietrzak, W. Simons, H. Cui, R. Riva, M. Naeije, A. Terwisscha van Scheltinga, E. Schrama, G. Stelling, and A. Socuet (2013), Importance of horizontal seafloor motion on tsunami height for the 2011 M_w = 9.0 Tohoku-Oki earthquake, *Earth Planet. Sci. Lett.*, *261*, 469–479.
Horspool, N., I. Pranantyo, J. Griffin, H. Latief, D. H. Natawidjaja, W. Kongko, A. Cipta, B. Bustaman, S. D. Anugrah, and H. K. Thio (2014), A probabilistic tsunami hazard assessment for Indonesia, *Nat. Hazards Earth Syst. Sci.*, *14*, 3105–3122.
Ichinose, H., Y. Hamano, K. Baba, and T. Kasaya (2013), Tsunami source of the 2011 Tohoku earthquake detected by an ocean-bottom magnetometer, *Earth Planet. Sci. Lett.*, *382*, 117–124.
Iwasaki, T., and A. Mano (1979), Numerical simulation of two-dimensional tsunami run up by Euler's coordinates, in *Proceedings of the 26th Japanese Conference on Coastal Engineering* [in Japanese], pp. 70–74.
Japan Society of Civil Engineers (JSCE) (2002), Tsunami assessment method for nuclear power plants in Japan, Tokyo, Japan. [Available at http://committees.jsce.or.jp/ceofnp/node/5.]
Kagan, Y., and D. D. Jackson (2013), Tohoku earthquake: A surprise?, *Bull. Seismol. Soc. Am.*, *103*, 1181–1194.
Kaiser, G., L. Scheele, A. Kortenhaus, F. Løvholt, H. Römer, and S. Leschka (2011), The influence of land cover roughness on the results of high resolution tsunami inundation modeling, *Nat. Hazards Earth Syst. Sci.*, *11*, 2521–2540.
Kajiura, K. (1963), The leading wave of a tsunami, *Bull. Earthquake Res. Inst.*, *41*, 535–571.
Koshimura, S., T. Oie, H. Yanagisawa, and F. Imamura (2009), Developing fragility functions for tsunami damage estimation using numerical model and post-tsunami data from Banda Aceh, Indonesia, *Coastal Eng. J.*, *51*, 243–273.
Lavallée, D., P. Liu, and R. J. Archuleta (2006), Stochastic model of heterogeneity in earthquake slip spatial distributions, *Geophys. J. Int.*, *165*, 622–640.
Løvholt, F., G. Pedersen, S. Bazin, D. Kuhn, R. E. Bredesen, and C. Harbitz (2012), Stochastic analysis of tsunami runup due to heterogeneous coseismic slip and dispersion, *J. Geophys. Res.*, *117*, C03047, doi:10.1029/2011JC007616.
MacInnes, B. T., A. R. Gusman, R. J. Le Veque, and Y. Tanioka (2013), Comparison of earthquake source models for the 2011 Tohoku event using tsunami simulations and near-field observations, *Bull. Seismol. Soc. Am.*, *103*, 1256–1274.
Mai, P. M., and G. C. Beroza (2002), A spatial random field model to characterize complexity in earthquake slip, *J. Geophys. Res.*, *107*(B11), 2308, doi:10.1029/2001JB000588.
Mai, P. M., and K. K. S. Thingbaijam (2014), SRCMOD: An online database of finite-fault rupture model, *Seismol. Res. Lett.*, *85*, 1348–1357.
Mai, P. M., P. Spudich, and J. Boatwright (2005), Hypocenter locations in finite-source rupture models, *Bull. Seismol. Soc. Am.*, *95*, 965–980.
McCloskey, J., A. Antonioli, A. Piatanesi, K. Sieh, S. Steacy, S. Nalbant, M. Cocco, C. Giunchi, J. D. Huang, and P. Dunlop (2008), Tsunami threat in the Indian Ocean from a future megathrust earthquake west of Sumatra, *Earth Planet. Sci. Lett.*, *265*, 61–81.
Mori, N., and T. Takahashi (2012), The 2011 Tohoku Earthquake Tsunami Joint Survey Group, 2012. Nationwide post event survey and analysis of the 2011 Tohoku earthquake tsunami, *Coastal Eng. J.*, *54*, 1250001-1-27.
Mori, N., T. Takahashi, T. Yasuda, and H. Yanagisawa (2011), Survey of 2011 Tohoku earthquake tsunami inundation and run-up, *Geophys. Res. Lett.*, *38*, L00G14, doi:10.1029/2011GL049210.
Mori, N., D. T. Cox, T. Yasuda, and H. Mase (2013), Overview of the 2011 Tohoku earthquake tsunami damage and its relation to coastal protection along the Sanriku coast, *Earthquake Spectra*, *29*, S127–S143.
Mori, N., N. Yoneyama, and W. Pringle (2015), Effects of the offshore barrier against the 2011 off the Pacific coast of Tohoku earthquake tsunami and lessons learned, in *Post Tsunami Hazards: Restoration and Reconstruction*, edited by V. Santiago-Fandino, Y. A. Kontar, and Y. Kaneda, pp. 121–132, Springer International Publishing, Springer, Switzerland, doi:10.1007/978-3-319-10202-3_9.
Murata, S., F. Imamura, K. Katoh, Y. Kawata, S. Takahashi, and T. Takayama (2010), *Tsunami: To Survive From Tsunami*, 316 pp., World Sci., Hackensack, N. J.
Murotani, S., K. Satake, and Y. Fujii (2013), Scaling relations of seismic moment, rupture area, average slip, and asperity size for M∼9 subduction-zone earthquakes, *Geophys. Res. Lett.*, *40*, 5070–5074, doi:10.1002/grl.50976.
Okada, Y. (1985), Surface deformation due to shear and tensile faults in a half-space, *Bull. Seismol. Soc. Am.*, *75*, 1135–1154.
Pang, A. (2008), Visualizing uncertainty in natural hazards, *Risk Gov. Soc.*, *14*, 261–294.
Pardo-Iguzquiza, E., and M. Chica-Olmo (1993), The Fourier integral method: An efficient spectral method for simulation of random fields, *Math. Geol.*, *25*, 177–217.
Razafindrakoto, H. N. T., P. M. Mai, M. G. Genton, L. Zhang, and K. K. S. Thingbaijam (2015), Quantifying variability in earthquake rupture models using multidimensional scaling: Application to the 2011 Tohoku earthquake, *Geophys. J. Int.*, *202*, 17–40.
Reese, S., B. A. Bradley, J. Bind, G. Smart, W. Power, and J. Sturman (2011), Empirical building fragilities from observed damage in the 2009 South Pacific tsunami, *Earth Sci. Rev.*, *107*, 156–173.
Satake, K., Y. Fujii, T. Harada, and Y. Namegaya (2013), Time and space distribution of coseismic slip of the 2011 Tohoku earthquake as inferred from tsunami waveform data, *Bull. Seismol. Soc. Am.*, *103*, 1473–1492.
Shuto, N. (1991), Numerical simulation of tsunamis—Its present and near future, *Nat. Hazards*, *4*, 171–191.

Somerville, P. G., K. Irikura, R. Graves, S. Sawada, D. J. Wald, N. A. Abrahamson, Y. Iwasaki, T. Kagawa, N. Smith, and A. Kowada (1999), Characterizing crustal earthquake slip models for the prediction of strong ground motion, *Seismol. Res. Lett.*, *70*, 59–80.

Suppasri, A., E. Mas, I. Charvet, R. Gunasekera, K. Imai, Y. Fukutani, Y. Abe, and F. Imamura (2013), Building damage characteristics based on surveyed data and fragility curves of the 2011 Great East Japan tsunami, *Nat. Hazards*, *66*, 319–341.

Tanioka, Y., and K. Satake (1996), Tsunami generation by horizontal displacement of ocean bottom, *Geophys. Res. Lett.*, *23*, 861–864.

Tappin, D. R., S. T. Grilli, J. C. Harris, R. J. Geller, T. Masterlark, J. T. Kirby, F. Shi, G. Ma, K. K. S. Thingbaijam, and P. M. Mai (2014), Did a submarine landslide contribute to the 2011 Tohoku tsunami?, *Mar. Geol.*, *357*, 344–361.

Thio, H. K., P. Somerville, and G. Ichinose (2007), Probabilistic analysis of strong ground motion and tsunami hazards in southeast Asia, *J. Earthquake Tsunami*, *1*, 119–137.

Yamazaki, Y., T. Lay, K. F. Cheung, H. Yue, and H. Kanamori (2011), Modeling near-field tsunami observations to improve finite-fault slip models for the 11 March 2011 Tohoku earthquake, *Geophys. Res. Lett.*, *38*, L00G15, doi:10.1029/2011GL049130.